Università degli Studi di Padova

Dipartimento di Fisica e Astronomia
"Galileo Galilei"

Corso di Laurea Magistrale in Fisica

Optimal Bounds on Heavy-Mediator Dark Matter

Relatori:
Dr. Andrea Wulzer
Prof. Marco Zanetti

Laureando:
Federico Pobbe

Anno Accademico: 2015/2016

Abstract

The aim of the thesis is to design a model-independent strategy for the interpretation of Dark Matter searches at colliders, using as a reference the CMS mono-jet analysis of the data gathered by the detector in 2015 at $L = 2.24 fb^{-1}$ and on its possible extension at $L = 100 fb^{-1}$. The strategy is based on an Effective Field Theory (EFT) description of Dark Matter that allows us to set bounds under the hypothesis that the Dark Matter interactions are due to the exchange of heavy mediator particles. Implementing it in a concrete experimental situations and assessing the expected limits requires a detailed study of the background and a refined simulation of the signal. Moreover, a new statistical procedure, based on the Shape Analysis method, is introduced in order to set universal bounds on heavy-mediator Dark Matter production at LHC. A comparison is performed between the performances of the new statistical method and those of a more traditional Cut and Count strategy. EFT limits can be reinterpreted in any specific underlying model.

CONTENTS

INTRODUCTION

Understanding the nature of Dark Matter is one of the main goal in the physics research of the twenty first century not only from a cosmological point of view. The theoretical models that describe the nature and the interaction of the Dark Matter with other particles are many, as the experimental approaches that aim at proving its existence. The lack of knowledge about what the Dark Matter actually consists of led to the proliferation of different models; testing each of them experimentally is practically unfeasible. Therefore, a model independent strategy is necessary to assess the real nature of Dark Matter.

The first evidences for the existence of the Dark Matter dates back to the beginning of the twentieth century, when the first observation of the unusual motion of the galaxies and clusters led to the conclusion that there is a discrepancy between the mass we can directly observe and the actual mass of the Universe. The hypothesis of a new kind of particle beyond the Standard Model which is stable on cosmological scales and that have nearly no interaction with the ordinary matter is one of the most corroborated possibilities. The abundance of the Dark Matter is well explained by a thermal freeze-out mechanism in the early universe, which leads to the so called WIMP (Weakly Interacting Massive Particle)-miracle, the coincidence between the current Dark Matter density and the strength of the interaction these particle must have with the ordinary matter to reproduce the abundance. However, the conditions to reproduce the WIMP-miracle are not so strict and, as a consequence, the possible models implementing this "miracle" are many.

The necessity of a model-independent approach justifies the usage of an Effective Field Theory (EFT). An EFT is a low-energy approximation of a complete model (UV model) which is easier to test, but that presents a limited range of validity. The key features of the EFT approach are that a single effective operator can be generated by many different models and that, for a given maximal energy dimension, the number of possible operators is finite and reasonably small. The EFT approach is used to set bounds or to constrain the microscopic underlying model. The limit-setting strategy within the EFT and the accuracy of the bounds depends strongly on the performance of the statistical method adopted to interpret the experimental data. Usually, the statistical procedures in these situations are based on the fact that the signal predicted by the EFT underestimates systematically the true signal because of its range of validity. The

statistical interpretation of this property leads to an exclusion bound on the parameters of the EFT, which can be reinterpreted in any specific microscopic model.

The aim of this thesis is to provide a model-independent interpretation to set bounds on the parameters of the EFT adopted to describe the Dark Matter production at the Large Hadron Collider (LHC). The 2015 CMS mono-jet analysis is used as reference for the implementation and discussion of this limit-setting strategy. Accurate simulations are performed to reproduce the signal and the background for the statistical analysis. The work is focused on the statistical methods to extract these bounds. The property of underestimation of the true signal is straight forwardly implemented in the cut and count method (compare data counts with expectation in a predefined phase space region), which consists in imposing that the signal predicted by the EFT is less than the maximum allowed signal according to the background in an optimised signal region. To increase the statistical power of the analysis, the distribution of the events predicted by the EFT can be interpret as a lower bound on the true signal distribution. However, the implementation of this kind of method is not as intuitive as the cut and count, so a dedicated analysis is required to understand how this procedure can be properly implemented. The performances of the two procedures are tested to choose which one provides the stronger bounds.

The content of this thesis is divided into four chapters. In chapter 1, we introduce the details of the EFT we decided to adopt to describe the Dark Matter interaction with the standard model particles. Moreover, we will describe the different possible methods for the detection of Dark Matter, focusing on the collider search performed by the CMS experiment at LHC. In chapter 2, we describe how we can use the dedicated softwares at our disposal to reproduce the background and to simulate the EFT signal using the CMS mono-jet analysis as reference. In the last section of the chapter we will discuss the event selection and the efficiencies. In chapter 3, we introduce and discuss in details the statistical procedures adopted for the limit-setting strategy, focusing on the second method which is the original contribution of this work. In chapter 4, we discuss the results obtained and compare the performance of the statistical procedures. Moreover, we will use the stronger bounds for a further analysis of the exclusion limits on the Dark Matter production. Finally, we will discuss the limits of our procedure and the possible improvements that can be made to obtain better results from the analysis.

CHAPTER 1

DARK MATTER @ LHC

Searching for Dark Matter is one of the main goals of the new run of the LHC experiment. The discovery of such kind of particles will be a step forward in fundamental physics research. Besides accounting for the cosmological and astrophysical evidence for dark matter, it will start the new research branch that can lead to a better comprehension of the fundamental structure of the universe. In the following chapter we will briefly motivate the introduction of this new kind of particle and we will describe the concept of Effective Field Theory applied to in this kind of analysis. Moreover, we will discuss the possibilities for the detection of this kind of particles, focusing on the collider search.

1.1 DARK MATTER EFT

Since the first proper observations of stars and galaxies have been provided, astronomers and astrophysicists noticed that there was something strange in the motion of the bodies. For example, stars, asteroids, planet and interstellar gas are not enough to explain the peculiar shape of the spiral galaxies. To explain the spiral structure, astronomers supposed the existence of a new kind of matter, which is opaque to the electromagnetic field, but that can interact gravitationally and then account for the strange behaviour of the galaxy. Many other cosmological and astrophysical studies seems to lead to the same conclusion: the universe is permeated by a gas of particles that can not be detected which determines the structure of the galaxies and clusters.

The first time the words "Dark Matter" [1–3] were used was in 1932, when Oort measured that the mass of the brightest stars in the Milky Way account for only one third of the approximated mass of the galaxy. In the following years, more precise observations inside and outside the galaxy confirmed the fact that the mass we see is less then the actual mass in the universe. For example, the deviations in the velocities of the globular clusters inside the Milky Way, observed by Kinman in 1959, suggested that the mass density increases linearly with the radius. Also the measure of the velocity of the galaxies in in the Coma cluster, made by Fritz Zwicky in 1933, led to the conclusion that

the mass contained in the cluster is hundred times the visible one. Finally, the extremely precise observations of the CMB (Cosmic Microwave Background) obtained by the Plank satellite [4] imply that the sum of dark matter and baryon energy densities over critical density $\Omega_m = 31.6\%$ and the energy density of the dark matter is 26.7% of the total one.

Another important example is the observation of the *Bullet Cluster* in 2006 [5]. This system is composed of two primary galaxy concentrations, which passed through each other $\simeq 100$ Myr ago. As result of the collision, the various components of the two galaxy clusters (dark matter, X-ray emitting plasma, and galaxies visible in the optical spectrum) underwent different interactions with the components of the other clusters. The ordinary matter slowed down during the collision because of its electromagnetic interaction, whereas the dark matter components passed through each other without significant consequences, in the hypothesis that they can interact only gravitationally or through a very weak self-interaction. Under this conditions, the outcome of the collision is a displacement between the barycenters of the hot gas distribution (visible X-ray spectrum) and the dark matter distribution (which can be observed by gravitational lensing). This observation is very important because such an effect is hard to explain without introducing the existence of dark matter particles.

A plausible and simple mechanism by which dark matter can have been produced during the cosmological evolution of the universe is the so called *Thermal Freeze Out* [6]. It is the simplest way to explain the abundance of a certain species in an expanding universe. If two particles X and Y can turn into each other through the reactions $XX \leftrightarrows YY$, in the early stages of the universe, when its temperature T is very high, the two species annihilate into each other maintaining the equilibrium. At a certain point the temperature T of the universe drops below the higher of the two masses, for example m_X. The consequence is that the number density n_X of X, in the hypothesis that X remains in thermal equilibrium, follows the non-relativistic Boltzmann distribution, which includes a suppression factor $e^{-\frac{m_X}{KT}}$. Hence, the particle X will annihilate into particles Y following the Boltzmann distribution.

Therefore, n_X should decrease to zero as the universe cools down, unless also the inverse reaction $XX \to YY$ is suppressed. This will happen because of the expansion of the universe, which dilute the concentration of the non-relativistic particles. When the annihilation rate of the reaction $XX \to YY$ decreases below the Hubble rate of expansion $H = \frac{\dot{a}}{a}$, where a is the scale factor of the Friedman-Robertson-Walker metric, the annihilation of X particles stops. As a consequence, the value of n_X is fixed.

This mechanism can be one explanation to the abundance of dark matter suggested by the cosmological observation. One support to he validity of the thermal freeze-out mechanism is the coincidence named *WIMP-miracle* [7, 8], where WIMP stands for Weakly Interacting Massive Particle. In a reaction of the kind described above (when we denote with X the dark matter particle) if we impose the ratio between the dark matter density and the critical density $\Omega_X \sim 0.3$ and we assume that X is weakly coupled to Y, we obtain that the mass of the particle X must be in the range of 1-1000 GeV. This

coincidence is very difficult to ignore. Another important point in this result is that the abundance of the particle X mostly depends to the cross section of the annihilation process while the sensitivity to the mass m_X is rather mild. This is the reason why the mass range for the dark matter particles is so wide. Moreover, this mechanism is independent from the early thermal history of the universe and of the interactions at high energy scales.

These assumptions lead to requirements for dark matter. The dark matter particle should be stable on cosmological scales and in thermal equilibrium in the early universe, it should annihilate to other particles and the corresponding cross section must be low-limited to avoid over abundance. The conditions imposed by the WIMP miracle are very general and, as a consequence, plenty of models exist which account for dark matter and for its interaction with the Standard Model. It is difficult, or even impossible, trying to test each model individually within the possible experiments. In this work we will adopt the Effective Field Theory approach [10–23].

1.1.1 Effective Field Theory

An *Effective Theory* is an approximation of a complete model, where some degrees of freedom are integrated out in order to simplify the resulting theory. The consequence of this approximation is a limited range of validity. This "effective" approach is often used in particle physics when a certain reaction is mediated by a heavy particle, such as a massive vector boson, which is difficult to produce on shell because of the high mass. Therefore, the effective theory will be a low-energy approximation of the complete model, that will fail when the energy of the process reaches the mediator's mass scale. To make this kind of approximation, we suppose that the model can be separated in different energy scales. In the case of heavy-mediator models, the separation is usually determined by the mass of the mediator. Hence, when the energy of the process is lower than the mass of the mediator, we suppose that it can be described by an effective operator (Effective Field theory), whereas when the energy is equal or above the threshold, we need to know the complete model (Ultra Violet theory). Before discussing the model chosen for our work, we will briefly describe a famous example of EFT, the Fermi Theory of Weak Interaction [9].

Inside the Standard Model, the electroweak interaction is described by the existence of four vector bosons, associated to the $SU(2)_L \otimes U(1)_Y$ gauge symmetry group and to the Symmetry Breaking mechanism of the Higgs boson. One boson is neutral and massless and correspond to the photon γ, whereas the other three bosons have a mass, the Z^0 is neutral, the W^+ and W^- and charged with respectively $M_Z = 91$ GeV and $M_W = 80$ GeV. The photon is responsible for the electromagnetic interactions among charged particles, while Z^0 and the W account for the weak interaction processes such as the muon decay $\mu^- \to e^- \bar{\nu}_e \nu_\mu$ depicted in fig. 1.1.

The total centre of mass energy E_{CM} of the decay process coincides with the muon

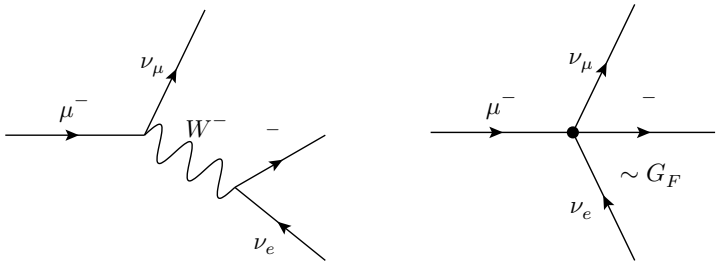

Figure 1.1: The figure shows the Feynman diagrams describing the weak muon decay with the complete lagrangian (left panel) and with the effective approximation (right panel)

mass m_μ, which is 106 MeV. The process occurs through weak interactions, but E_{CM} is too low for the W^- boson to be produced on shell. As consequence, in this kind of processes we do not need to use the full Standard Model lagrangian, but only an approximated effective interaction operator that mimics the effect of the weak force at the energy scales below the W boson mass.

The result is a vertex operator where the degrees of freedom of the mediator do not appears. Figure 1.1 shows the Feynman diagrams corresponding to the muon decay in the complete model (left panel) and in the effective theory approximation (right panel). As we can see, in the diagram of the effective theory the W boson propagator does not appear. This lead to a simplify description of the process. Moreover, the absence of the mediator in the effective vertex makes it independent of the detailed properties of the W boson which are present in the complete SM lagrangian. It depends only on the particles involved in the process ($\mu^-, \nu_\mu, \bar{\nu}_e, e^-$) and on the effective coupling constant G_F. This means that the effective model can be tested separately from the underlying UV theory. This means for instance that we can measure with good accuracy the value of the coupling constant G_F and of the masses of the particles involved in the process. Even though it is not the complete theory, the Fermi operator is currently used to study the weak processes in the low energy regime, such as β-decays.

The determination of G_F through the measurement of these low energy processes helped also to constrain the value of the parameter of the full Standard Model lagrangian. The value of the effective coupling G_F fixes the relation between the microscopic coupling constant g_W and the mass of the W boson M_W. The relation is:

$$G_F = \frac{g_W^2}{2M_W^2} \tag{1.1}$$

Hence, we can obtain a constraint on the value of the parameters of the underlying model testing its low-energy approximation. In eq. 1.1 we see that the effective coupling constant carries the dimensionality of a mass squared $[G_F] = M^{-2}$. From this simple

observation we can deduce, by a dimensional analysis, that the effects of this kind of interaction are small at low energies. A dimensionless parameter to test the interaction strength is $G_F E^2$, where E is the energy of the process. If the energy regime is low, $G_F E^2 \ll 1$, and the strength of the interaction operator is weak. On the other hand, when the energy of the process increases, the product $G_F E^2$ becomes order one or bigger and the theory starts approaching a strong coupling regime where it becomes non perturbative and thus it loses its applicability.

For the decay processes of relatively light particles, when the energy is always fixed to the mass of the particle that decays, there is no need to introduce the full UV model. However, for processes where the centre of mass energy can take a wide range of values, such as the collisions, it is important to determine which is the range of validity of the effective model. For example, we can consider the electron-positron annihilation into muons ($e^+e^- \to \mu^+\mu^-$). If the process takes place at a centre of mass energy $\sqrt{s}$ lower than the mass of the Z boson, we can describe it accurately using the Fermi Theory (plus of course electromagnetism, which gives the main contribution at low energy). As the energy $\sqrt{s}$ approaches the value of M_Z, the cross section increases because of the resonant production of the Z. This effect is not predicted by the EFT and we should shift to the full lagrangian for a proper description. All this considerations stress the fundamental fact that an EFT is not a complete model, but only and approximation and it is important, then, to worry about its range of validity before using it to make predictions.

In light of the above considerations concerning the model-independence and the effectiveness of the EFT approach, we will exploit it to describe the dynamics of the dark matter particle and in particular its coupling to Standard model particles which is responsible for LHC production. The latter interactions can be universally described, in the appropriate kinematical regime, by a low-energy EFT Lagrangian, invariant under the SM gauge group and the Lorentz group:

$$\mathcal{L}_{EFT} = \mathcal{L}_{SM} + \mathcal{L}_X + \mathcal{L}_{int} \tag{1.2}$$

where $\mathcal{L}_{SM}$ is the Standard Model lagrangian, $\mathcal{L}_X$ is the free-lagrangian of the dark matter particles and $\mathcal{L}_{int}$ contains the operators describing the dark matter interactions with the ordinary matter. The form of the operators in $\mathcal{L}_{int}$ is universal and the lack of information we have about the complete model does not prevent us from studying them by treating the coefficients as free parameters. It will be possible to compute their values only once the underlying theory will be discovered. The allowed operators in $\mathcal{L}_{int}$ can be classified according to their mass dimension d and, for each fixed d, their number is finite and reasonably small. In this work, we will consider operators with $d = 6$, assuming, as it is often the case, than lower dimensional operators are forbidden by symmetries or small. Therefore, $\mathcal{L}_{int}$ can be parameterized as follows:

$$\mathcal{L}_{int} = \frac{1}{M_*^2} \sum_i c_i O_i \tag{1.3}$$

where the sum runs over all $d = 6$ operators O_i allowed by the symmetries, c_i are dimensionless coefficient and the effective coupling strength is parameterized by $G_X = 1/M_*^2$.

Specifying the lagrangian is not enough for a complete operative definition of the EFT. As we saw in the Fermi example, we still need to specify its maximal range of applicability, above which it stops giving trustable predictions. We call this parameter the EFT *cut-off* M_{cut} and we stress that it should be regarded as a completely free parameter from the EFT point of view. From the view point of the underlying UV theory, M_{cut} is associated with the mass of the heavy mediator.

The free parameters of the EFT that we will consider in our model are the following:

- the mass of the dark matter particle m_{DM}
- the energy scale of the theory M_*
- the cutoff scale M_{cut}

For the present work, we assume that the dark matter particle is a Majorana fermion, singlet under the Stardard Model gauge group and represented by a self-conjugated four-component spinor $X = X^c$. The choice of using Majorana fermions is motivated by the requirement for the dark matter to be neutral and by the fact that in the Standard Model the particles that describe the ordinary matter (leptons and quarks) are all fermions. However, this is not the only hypothesis. For example, for a similar analysis we can suppose the dark matter to be described by Dirac fermions. Under these assumptions, the free lagrangian takes the form:

$$\mathcal{L}_X = \frac{1}{2} \bar{X} (i\gamma^\mu \partial_\mu - m_{DM}) X \tag{1.4}$$

and the effective operator we will chose to study as an illustrative example is an axial-axial four fermion interaction of $d = 6$:

$$\mathcal{L}_{int} = -\frac{1}{M_*^2} (\bar{X}\gamma^\mu\gamma^5 X)(\sum_q \bar{q}\gamma_\mu\gamma^5 q) \tag{1.5}$$

where the sum is over all quark flavours (q = u, d, c, s, b, t). In the equation, the dimensionless coefficient c has been re-absorbed in the definition of M_* and the overall

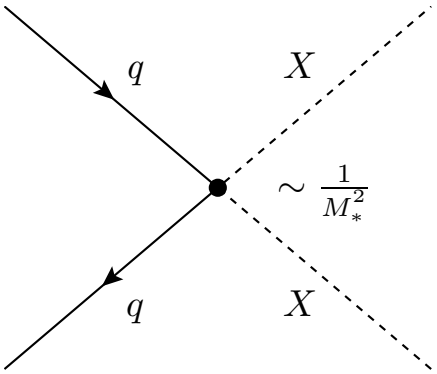

Figure 1.2: Interaction vertex corresponding to the interaction lagrangian we assumed to test.

minus sign is purely conventional. The interaction vertex originated by the operator in 1.5 is shown in fig. 1.2.

Notice that this effective operator may have many different microscopic origins. For example, in [24] are described two possible simplified models which are effectively approximated by this operator in the low energy regime. As a consequence, this simplification is very useful in order to set bounds on the possible interactions that dark matter can have with the Standard Model particles.

When discussing our EFT for DM, we emphasized that the parameters M_* and M_{cut} are completely independent and no relation must be assumed between the two. However, they can be related with the underlying UV theory, as it happens in the Fermi Theory. In that case there is a particular relation between the effective coupling G_F and the mass of the heavy mediator M_W, namely they are related by the coupling constant g_W as in 1.1. The same could happen in our dark matter model, in which case M_* and M_{cut} are related by:

$$M_{cut} = g_* M_* \tag{1.6}$$

where g_* is a suitably defined coupling strength of the complete model. With a simple algebraic manipulation we get:

$$G_X = \frac{1}{M_*^2} = \frac{g_*^2}{M_{cut}^2} \tag{1.7}$$

Comparing this result with 1.1 we can identify the cut-off scale M_{cut} with the mass of the heavy mediator of the possible microscopic models. We will use this relation for reporting limits on dark matter in a convenient format. This relation will provide an interesting result in the exclusion limit-setting.

In the following section, the most important experimental approaches to dark matter detection will be discussed. We will also introduce the problems in the use of our EFT depending on the type of experiment we choose.

1.2 Dark Matter Detection

According to the assumption of the Freeze-out mechanism in the early universe, we can say that dark matter particles must couple weakly to some of the other particles of the universe, apart from the gravitational interaction. In particular, in a WIMP-like scenario, we suppose the existence of an interaction between dark matter and the standard model on the weak scale. Therefore, the possibility to detect these particles with experiments is justified. The possible strategies that can be adopted to detect Dark Matter particles are three, *Direct*, *Indirect* and *Collider* search. In fig. 1.3 the schematic Feynman diagrams that characterize the three different type of experiments are shown.

Direct Searches [1, 25] try to detect the motion of the Earth through the dark matter distribution of our galaxy. It is based on the assumption that the particle of the so called "dark matter wind" can, although weakly, interact with the nuclei of the ordinary matter. The search is carried out monitoring a large detector made of a specific high-density material in order to maximise the cross section of the process. The expected signal is very low, therefore the cosmic rays or other sources of background have to be minimised. One possible solution often adopted in this cases is to put the detector underground, in a mine or inside a mountain.

The second possibility is to use the *Indirect* [2, 3] approach, which consists in searching for the radiation emitted by processes of dark matter annihilation in the universe. Indeed, the reactions which produced dark matter in the early universe are now inefficient and their impact of the dark matter density is negligible, but this does not mean that they can not take place in the present universe. The rate of dark matter annihilation is proportional to the square power of the dark matter density ($\Gamma_{ann} \propto \rho^2_{DM}$), so in order to

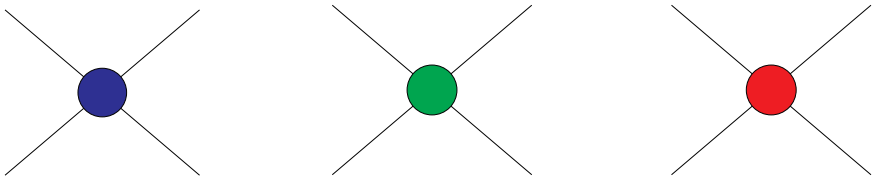

Figure 1.3: The figure shows the schematic Feynman diagrams involved in the three kind of searches for Dark Matter. With "X" we refer to the DM particle, while with "SM" we mean a particle of the Standard Model. We suppose the time to flow from left to right.

maximise the probability of detecting the radiation produced by the annihilations, the telescopes must look at the regions where the dark matter accumulates, such as galactic centres.

The third approach to the dark matter detection is the *Collider Search*. As the direct search, it is based on the assumption of a weak interaction between the dark matter and the ordinary matter, with the difference that in this case we suppose to produce the DM pair with high-energy collisions. Because of the extremely weak interaction with the ordinary matter, DM is expected not to leave any track in the detectors. As a consequence, its experimental signature is a rather large amount of *Missing Energy* with an additional trigger required, such as a jet. In hadron colliders, the energy of the reactions is unknown, so we will refer to the *Missing transverse Energy* [1] , namely the missing energy calculate in the transverse plane with respect to the beam.

A usual requirement about dark matter particles is to respect a discrete $\mathbb{Z}_2$ parity. The reason for this condition is the stability of the dark matter on cosmological scales. It is very unlikely that a massive particle with a weak-like interaction does not have a decay channel, unless some discrete symmetry which gives a different quantum number to the observable and the dark matter sector is preserved. In that case, the lightest particle with a given quantum number for that symmetry is absolutely stable. Moreover, this implies that the dark matter particles can only be produced in pairs.

While the processes studied by the direct and indirect searches take place at a safe low E_{CM}, the energy of the collisions in a collider can be of the same order or even higher than the cut-off scale M_{cut}. Therefore, in our analysis, we need to take into account the possibility that the prediction of our effective model may fail.

In this work we will consider only the third category of experiments. We will suppose to test our dark matter EFT model within the CMS experiment at LHC. In the following section we will give a brief description of the detector. We will explain why this specific detector is suitable for our purpose and how actually the production of dark matter can be detected.

1.3 THE CMS EXPERIMENT

As we said in the previous sections, our limit-setting analysis for the EFT dark matter will apply to the measurements at collider experiments. We will use as a reference the data obtained from the *Compact Muon Solenoid* detector, one on the main four experiment of at LHC. The Large Hadron Collider LHC [26] is a proton-proton and heavy-ion collider operating at CERN since 2009 in the 27 km tunnel previously used by the LEP electron-positron collider. The choice of a non elementary particle, as the proton, for the beams is dictated by the necessity to increase the energy of the collision. The centre of mass energy $\sqrt{s}$ of the proton beam was 8 TeV in Run I and now it is increased to 13 TeV.

[1] The Missing Energy is defined minus the vectorial sum of the momenta of the final states particles $\not{E} = -|\sum_i \mathbf{p}_i|$. In the case of hadron colliders the definition is $\not{E}_T = -\left|\sum_i \mathbf{p}_i^T\right|$)

In a proton-proton collider the energy of the reactions can not be constrained because of the nature of the protons. However, the machine can span a large range of interaction energy that makes it suitable for the search of new particles. The LHC beams collide in four different interaction points, where the four experiments take place. The *CMS* and the *A Toroidal LHC Apparatus (ATLAS)* are multipurpose detectors, designed around the experimental requirements to provide sensitivity to the search of new particles. The *LHC beauty (LHCb)* experiment is focused on the physics of the quark b, while *A Large Ion Collider Experiment (ALICE)* is designed to study the quark-gluon plasma produced in heavy ions collisions.

The LHC beam is split in more then 3000 bunches (2400 in 2015), 25 ns away from each other. The corresponding bunch crossing rate is thus about 40 MHz. Each bunch is composed by 10^{11} protons, and has a transverse size of 10 μm at the interaction point. As a consequence, the number of proton-proton collisions per bunch-crossing (*Pile-Up*) can be very high, 40 on average during Run I and about 25 in the first 13 TeV Run. The pile-up represents a great experimental challenge, particularly for the reconstruction and measurement of the $\not{E}_T$ and jets.

1.3.1 The Detector

For the purpose of this work, the CMS detector is used as reference, i. e. the simulations described in chapter 2 aim at reproducing the CMS performance in terms of efficiency and resolution of the various physics objects.

The CMS detector, shown in fig. 1.4, is a multi-purpose apparatus designed to study high-p_T physics processes in proton-proton collisions. It is 21.6 m long, 15 m wide and it weights about 12'500 tons. A superconducting solenoid occupies its central region, providing a magnetic field of 3.8 T parallel to the beam direction [28]. Charged-particles trajectories are measured by the silicon pixel and strips trackers, which cover a pseudorapidity region of $|\eta| < 2.5$. A lead tungstate ($PbWO_4$) crystal electromagnetic calorimeter (ECAL) [31, 32] and a brass/scintillator hadron calorimeter (HCAL) [33] surround the tracking volume and cover $|\eta| < 3$. A peculiarity of this detector is that the tracker and both the calorimeters are placed inside the solenoid. The steel / quartz-fiber Cherenkov hadron forward (HF) calorimeter extends the coverage to $|\eta| < 5$. Outside of the solenoid is placed the muon system [34, 35], which consists of gas-ionization detectors embedded in the steel flux return yoke and covers $|\eta| < 2.4$. The great coverage provided by the detector structure in addition to the tracking system makes it suitable for the search of new particles, such as dark matter candidates. Indeed, the hermeticity of the detector is fundamental for the analysis of events requiring a large amount of $\not{E}_T$, for obvious reasons.

The CMS detector deals with this high number of events with a *Trigger System* [37] which can select samples of relevant events with a rate of a few hundred Hz. We are

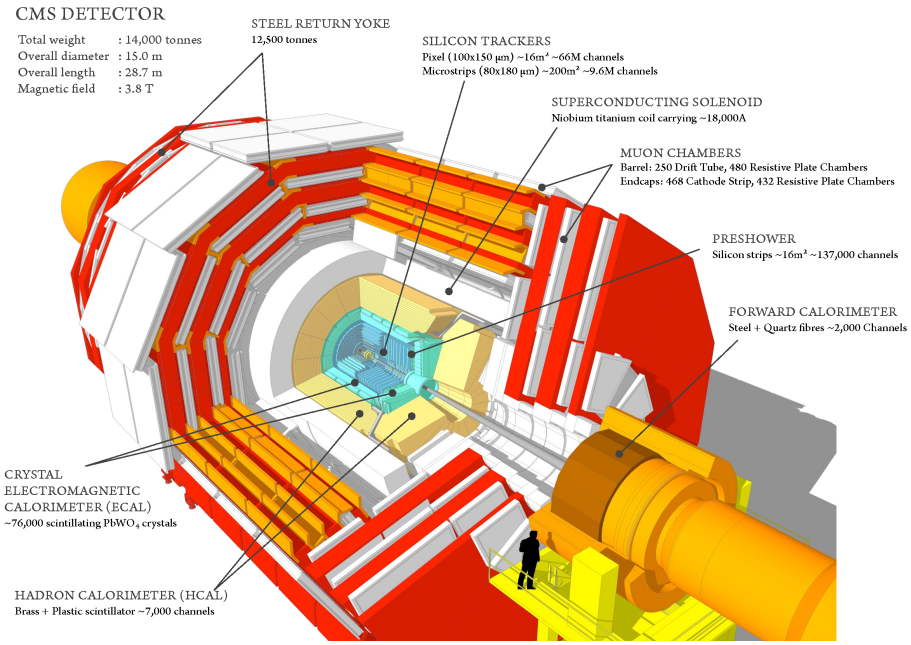

Figure 1.4: Detailed figure of the CMS detector

interested in events with a large amount of $\not{E}_T$, so the details of the jet-p_T and $\not{E}_T$ trigger will be briefly discussed.

The CMS online trigger system is divided into two levels. The first level is more general and requires an $\not{E}_T$, calculated only with the calorimeters, greater than 120 GeV. The second level trigger is dedicated to the mono-jet event selection, it requires the $\not{E}_T$, calculated now after the muon tagging, greater than 95 GeV, the leading jet transverse momentum p_T to be greater than 80 GeV and the pseudo-rapidity $|\eta| < 2.6$. As we said before, the reason of this online selection is that it is impossible to store the data of all the events provided by LHC and study them off-line. Fig. 1.5 shows the efficiencies of the trigger depending on the $\not{E}_T$ value for a preliminary analysis of the 13 TeV run. As we can notice, the efficiency reaches its maximum at $\not{E}_T = 200$ GeV and then remains stable. Therefore, the off-line selection will imply a cut-off on the missing energy at 200 GeV to have the maximum trigger efficiency. Similar considerations are made for all the other observables.

As regards the $\not{E}_T$ reconstruction and the jet-p_T measurements, the performance of the detector and the reconstruction algorithms are reported in 1.6. The plot refers to the 2012 $\sqrt{s} = 8$ TeV run of LHC, but we can use them as benchmarks for the current 13 TeV run. Indeed, as we said before, these uncertainties depends on the pile-up, namely a higher rate of collisions will make more difficult for the algorithm to reconstruct properly a single event. Since in 2012 the pile-up was about 50, the current uncertainties are surely

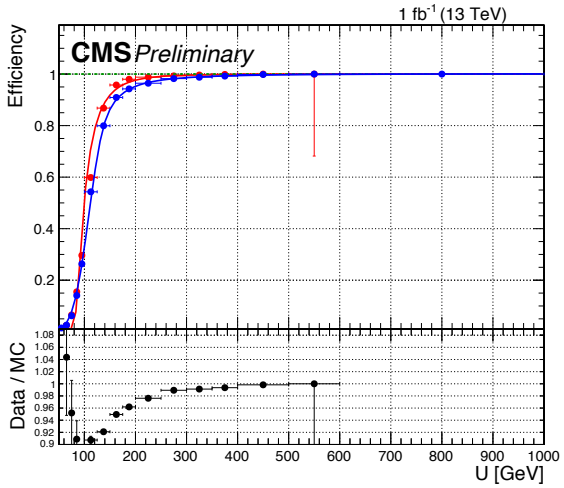

Figure 1.5: The figure shows the secondary trigger "turn-on" curve for the $U = \not{E}_T$ cut [39]. The blue curve corresponds to the $\not{E}_T$ trigger set to 120 GeV while the red curve to the 90 GeV trigger.

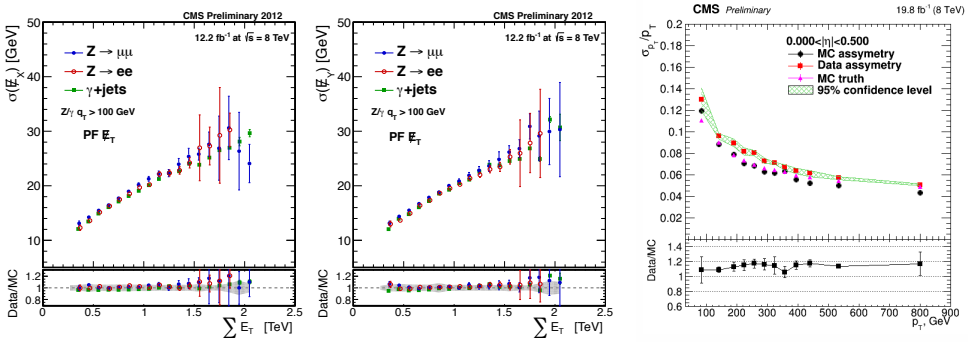

Figure 1.6: The figure shows shows the uncertainties of the reconstruction algorithms fot the $\not{E}_T$ (left and central panel)[40] and jet-p_T (right panel) [41]. The performance refers to the $\sqrt{s} = 8$ TeV run of 2012.

lower than in the previous run. In the left and central panel the uncertainty on the $\not{E}_T$ reconstruction is displayed. As we can see, the error increases with the total transverse energy. The jet-p_T uncertainty (right panel) has the opposite behaviour, it decreases as the jet become more energetic.

1.3.2 Mono-jet Event Signature

In the previous sections, we touched upon the fact that because of the extremely weak interaction with ordinary matter, dark matter is expected not to be seen by the detector. Therefore, its experimental signature is a high value of $\not{E}_T$, namely the "missing" momentum in the transverse plane. This condition is not enough for this kind of event to be detected, so the usual analysis for dark matter searches requires an extra jet with high transverse momentum $\mathbf{p}_T$ or an extra photon with the same characteristics.

For the present work we will consider only the mono-jet category, which at hadron colliders gives stronger limits than the mono-photon search. In addition to the $\not{E}_T$ we require the presence of a high-$\mathbf{p}_T$ jet (usually due to an energetic quark or a gluon in the initial state radiation) [36–39]. Besides the selection of events with high $\not{E}_T$ and an energetic jet, the goal of this cuts is to suppress the QCD background and to reject events with isolated leptons coming from the hard scattering.

The main Standard Model background for this category of events is due to the Z boson production and decay into two neutrinos with an initial state radiation (ISR) of a jet. In principle, in an e^+e^- collider this background can be reduced by tuning the energy of the collision far from the resonant production of the Z. Unfortunately this can not be done at LHC, which is an hadronic collider, and the energy of the reactions can not be constrained. Another important source of background is the W production plus ISR that decays into a neutrino and a lepton. If the lepton is not detected, the event is labeled as mono-jet.

The detailed condition for an event to be labeled as mono-jet are listed below.

1. The event must have at least one jet with $p_T > 150$ GeV and $|\eta| < 2$.

2. There must be $\not{E}_T > 200$ GeV.

3. There can be a second jet with $\Delta\phi(j_1, j_2) < 2$, $p_T > 30$ GeV and $|\eta| < 2.5$.

4. Events with μ or e with $p_T > 10$ GeV or $|\eta| < 2.5$ are rejected.

where $\Delta\phi(j_1, j_2)$ is the angle in the transverse plane between the two jets. Events with three or more jets are rejected. As we said before, in a proton-proton collision the SM process with the highest cross section is the QCD di-jet, where two jets are produced

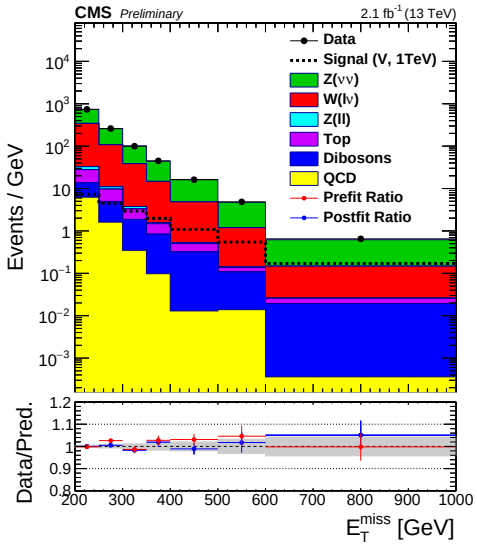

Figure 1.7: CMS mono-jet background for an integrated luminosity of $2.1 fb^{-1}$ and $\sqrt{s} = 13$ TeV [39]

back to back. This kind of event can affect the mono-jet selection because if one of the two jets is badly reconstructed and the p_T is underestimated it can generate $\not{E}_T$. The requirement of the point 3 accounts for this problem, excluding the events where the two jets are distant in the (ϕ, η)-plane.

Fig. 1.7 shows the mono-jet background at $\sqrt{s} = 13$ TeV for an integrated luminosity of $2.1 fb^{-1}$. As we can see, the QCD background is strongly reduced. The main components of the remaining background are Z($\nu\nu$) and W(νl) as we expected. Moreover, the graphic shows the great agreement between the Monte Carlo simulation of the components of the background (stacked histogram) with the data gathered by the detector (black points). The Monte Carlo simulation are tuned by the observation of similar processes in *Control Regions*. For example, to study the Z($\nu\nu$) background the simulations are based on the similar process Z($\mu^+\mu^-$). The study of this process is used to tune the parameters of the Monte Carlo simulations of Z($\nu\nu$). As expected, the $\not{E}_T$ distribution of the background events is a power-law.

We will base the background simulation for our analysis, described in the following chapter, on the result presented in this preliminary work. We will simulate only the Z($\nu\nu$) and W(νl), which account for more than the 90% of the total background. We will interpret the data in fig. 1.7 also to extract reasonable values for the background errors, which, as we will see, are fundamental for the statistical analysis and for the limit-setting procedure.

We report the result of the preliminary CMS analysis for the interaction between two

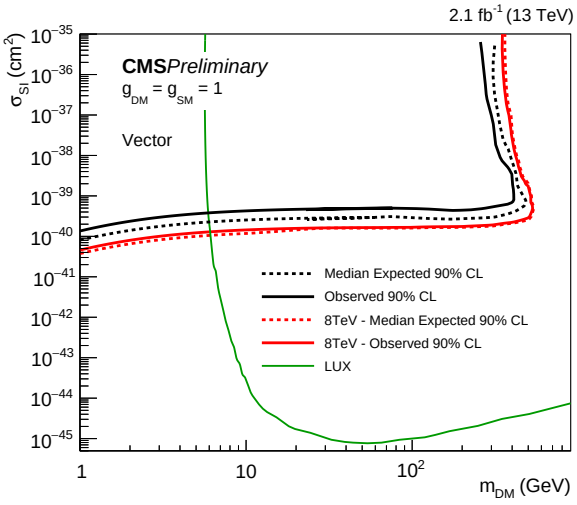

Figure 1.8: Dark Matter production cross section limits (90% C.L.) of the preliminary CMS analysis [39]

partons and two dark matter particles in fig. 1.8 . The bound is expressed as limit on production cross section depending on the dark matter mass. In the following chapters, we will present a new interpretation of the data of 1.7 in order to provide stronger bounds on the dark matter production at LHC.

CHAPTER 2

SIGNAL AND BACKGROUND SIMULATION

As we will see in the following chapter, the calculation of the parameters we need to know would require the the complete knowledge of the CMS data, which is not at our disposal for this work. Therefore, to perform our limit setting analysis on the dark matter EFT described in the previous chapter we need to obtain a data sample based on the true observation of the CMS detector. The simulated background must reproduce the distribution and the contribution of the different components, as we said in 1.3.2 . The accuracy of the simulation is fundamental to obtain more realistic results from our analysis. We choose to simulate our data sample (both background and signal) using some Monte Carlo based softwares.

However, it is not possible to use only one program to simulate the entire process from the proton-proton collision to the response of the detector, so we had to divide the process of simulation in three steps that at the end would give us the complete results. This three steps correspond to the phases of the collision and detection, namely the parton level process, the parton showering and hadronization, and the detector simulation. In the next sections we will discuss what these phases consist in, what are the simulators we decided to use for each step and how they work, and how we set the simulator's parameters to obtain the most realistic simulation of the process we described in the first chapter.

2.1 MONTE CARLO SIMULATIONS

2.1.1 The Parton-Level Process

We use the expression "parton level process" when we talk about the so called "hard scattering", namely the fundamental process which is supposed to be the origin of what we see in the detector. From the Standard Model we know that a proton is not

a fundamental particle, but it is composed by quarks and by *gluons*. For each process involving a proton-proton collision, the fundamental scattering is not the one between the protons, but the one between its constituents, called *partons*. This is the reason why we can not know which is the value of the invariant mass of the single event, a fact which will play an important role in what follows. In the case of Dark Matter production the starting point is the collision of two proton is seen as the combination of all the possible collisions between its components. We suppose that from this collision a pair of Dark Matter particles can be created according to the interaction vertex of the Effective Field Theory model we described in the first chapter.

Parton level events simulation were performed using *MadGraph*5 [42], an open source software written in Python. It can generate matrix elements at the tree-level for any Lagrangian based model, such as renormalizable or effective theories, implemented with FEYNRULES via the UFO interface[43]. After the process is specified by setting initial and final state particles, *MG*5 generates all Feynman diagrams of the process and produces the code needed to evaluate matrix elements at a given phase space point. The computer code obtained in this way can be then used for cross section calculations and events generation, via the MADEVENT package [44], which is included in *MG*5. The parameters used to simulate the sample in our case will be discussed later in this section.

MADEVENT is a parton level event generator which use Monte Carlo techniques to integrate the matrix element over the phase space and generate unweighted events, namely the number of events is proportional to the probability of areas of phase space. The algorithm used for the integration of the matrix element is called *Single-Diagram-Enhanced multi-channel integration*. Furthermore, the information about the generated events are stored in a code that can be passed to any shower Monte Carlo program for further showering and hadronization simulations. The specific information about the single events, such as the incoming and outgoing particle momenta, the spin of each particle or the QCD color, are also stored in a *Les Houches* file [45] so that the user can control and use them.

2.1.2 Parton Showering

After the hard scattering took place, the partons start to propagate, to decay and to interact with each other until their energy/momentum goes beyond a threshold and then they start to cluster together in hadrons. This stage of the evolution of the signal is called *parton shower* [47]. At this stage, QCD is still perturbative, but the complexity of the process does not allow to have a complete perturbative calculations beyond the next-to-leading order. In the shower process there are regions of the phase space where high-order terms are enhanced and must be considered. So, instead of aiming for a precise prediction to a fixed perturbative order, an approximate method that can take into account these enhancements will be preferred.

This method is called *parton branching* [47], and it is a recursive procedure that

leads naturally to its implementation with a Monte Carlo algorithm. This procedure is considered valid only for values of the squared transfered momentum t above a certain threshold t_0. For scales of $t < t_0$ this procedure must be combined with a non-perturbative model of the *hadronization* process. Suppose to have a process with a certain squared Feynman amplitude $|M_n|^2$ with an outgoing parton that branches in other two, for example a gluon that branches in two other gluons. We know that for a collinear emission of a parton the matrix element is enhanced, so our procedure must take it into account. The parton branching approximation allows us to write the squared Feynman amplitude of the process including the branching of the gluon $|M_{n+1}|^2$ in terms of the previous amplitude $|M_n|^2$. This approximation is permitted only if the angle between the two partons emitted is small, which is what we want to calculate according to the collinear enhancement. We consider now the effect of multiple branching. When we have more than one event of this type, we recombine all of this single branching processes in a single one equation called *evolution equation* which keeps the the enhancement of higher-order contributions associated with multiple small-angle parton emission. This is an equation for the *momentum fraction distribution* of the partons, which depends on the scale of the process (in our case on the squared transfert momentum t) and on the momentum fraction x. The evolution equation can be written in terms of the *Sudakov form factor* $\Delta(t)$ [47], which has a simple physical interpretation. The ratio $\frac{\Delta(t)}{\Delta(t')}$ represents the probability for a parton to evolve from t' to t without branching. The recursive structure of the parton branching an the probabilistic character of the evolution equation in terms of the Sudakov form factor make it easy to implement an algorithm using a Monte Carlo method.

The software we decided to use for the matching procedure is *Pythia 6.4* [48]. Pythia is a Monte Carlo based software that plays two fundamental roles in our simulation chain. Firstly, it works together with MG5/MADEVENT in the matching procedure.

2.1.3 Merging

As we said before, what we see in the detector is not the "hard scattering" process, but an event made mainly of jets which can be produced by a parton of the hard scattering, or by an extra jet created during the shower/hadronization . No factorization theorem exists to rigorously tag the type of the jet in the final state. Moreover, the existence of several hard scales, like the jet transverse energy or the di-jet invariant mass, which for a generic multi-jet event will span a wide range, makes more difficult to separate the two cases. So, if we want to reconstruct what the original process is starting from this jet tracks, we need an algorithm with the conditions to link the jets in the detector to partons created in hard process, the so called *"Merging scheme"* [46].

This merging, or matching, scheme contains the factorization prescriptions to establish if a given $(n+1)-$jet event is obtained from the collinear/soft-radiation evolution of an appropriate $(n+1)-$parton final state, or from an $n-$parton configuration where

hard, large-angle emission during its evolution leads to the extra jet. The condition for a merging scheme to be efficient are three. The first one is avoiding *double counting*, namely preventing an event to appear twice, each for every evolution path. The second one is avoiding *dead zones*, which means ensuring that each configuration is created by an allowed evolution path. The last one is optimizing the choice of the evolution path, in order to obtain the best approximation to the given kinematics.

The matching strategy is similar for each algorithm. The first step consists in defining the observables to describe a jet in the final state, such as the cross section or the transverse momentum. After this, a simulation of the parton level process is performed according to the matrix element. In our case this step is performed by *MG*5/MADEVENT and it is connected to what it was discussed in the previous section. The next step consists in accepting or rejecting the configuration with a probability depending on the dyamic and kinematic parameters set for the simulation. If the event is reject, the algorithm restart from the previous point. Finally, the simulator for the parton shower is invoked with the suitable initial conditions for each parton-leg according to the previous steps. The configurations that would have a higher jet multiplicity are vetoed in this step.

In our case, we selected three possibile parton-level processes with different number of parton legs. The matching scheme implemented in MG5/MADEVENT, while is generating the events, have to consider that they can be originated by one of these three processes and act as a consequence following the steps described before.

There are many merging schemes with different characteristics. For our purpose, we decided to choose the so called *"MLM"* scheme [46]. This algorithm uses a procedure based on the evaluation of some parameters of the phase space for each partonic event and the corresponding shower parton-shower generated by the showering algorithm in order to verify their compatibility. The variables involved are the transverse momentum of the $\mathbf{p_T}^{part}$, the pseudo-rapidity η^{part} and the distance in the (η, ϕ) plane ΔR_{jj} between two jets.

The conditions applied for the matching are the following:

$$p_T^{part} > p_T^{min}, \quad \eta^{part} < \eta^{max}, \quad \Delta R_{jj} > R^{min} \tag{2.1}$$

Now there happens the proper matching procedure. The algorithm starts selecting the hardest parton, and the jet, generated by the showering program, which is the closest in the (η, ϕ) plane. If the distance between the parton and the jet centroid is suitable the parton and the event *match*. The jet is removed from the list of jets, and then the algorithm does the matching test for the next parton. We can say that an event is fully matched if each parton matches a jet.

2.1.4 Hadronization

After the scale of the process goes below the cut-off scale t_0, we have a set of coloured partons with a virtual mass-square of the order of t_0. At this scale, QCD is no more perturbative, so we need a model to describe how this coloured particles are clustered into hadrons. We are going to describe the so called *String Model* of hadronization because is the one implemented in the software we used for the shower and hadronization simulation.

Once the partons are created, they start to spread out and lower their energy scale. For the properties of QCD, the coloured field between them grows stronger and stronger until it reaches the *string* configuration. After a certain energy/distance scale, the coloured string will be strong enough to create $q\bar{q}$ couples. At that point, there happens the fragmentation of the string and the consequent hadron creation. In the next section we will describe how this hadrons are collected together in jets and then become observable by the detector.

This stage of simulation is performed by Pythia, as the showering. After the parton-level process is generated by MG5, Pythia performs the parton-showering and do the matching to decide whether accept or reject an event. The hadronization process is performed on the survived events.

2.1.5 Detector Simulation

In the previous sections we discussed the evolution of the parton level process, the concepts of parton branching, showering and hadronization. At this stage of the simulation we have a file containing all the information about which hadrons are produced in the final state and about other particles, such as leptons and photons, that can appear in the final state of this processes. As we said in the first chapter, CMS is composed by a tracker, an electromagnetic calorimeter, a hadron calorimeter and the muon chambers. These components have a different response to the particles that flow through them. For example, hadrons leave are seen in the hadronic calorimeter mainly with the form of a jet, or muons firstly leave a track in the initial tracker and then in the muon chambers. These instruments have an efficiency though, so it can happen that some particles generated after the hard scattering may not be revealed. For example a muon that is generated with $\eta > 2.4$ will not be detected because that area is not covered by the muon chambers.

All these considerations have to be taken into account when a detector simulation is performed. We need a program which can take as input the result of the parton-level + shower + hadronization, simulate the response of the detector and create an output file with the information that we would obtain if we were performing the real experiment.

Before the description of the detector simulator we chose, the procedure of *jet reconstruction* must be discussed. When the hadrons hit the detector they must be clustered into a jet in order to link them the a parton of the hard scattering. There is not only one algorithm that can do this operation, so in order to get the best approximation, we must

choose the best cluster algorithm for our process. After the reconstruction, the jet is considered as a single particle with a fixed momentum.

For our purpose, it was decided to choose the *Anti-k_t* clustering algorithm [49]. This algorithm belongs to a family of jet-clustering procedures called k_t *algorithms*, which consists in all the algorithms that use as discriminant the transverse momentum, k_t, of the particles considered. Suppose we have two particles with momenta $\mathbf{p}_i$ and $\mathbf{p}_j$ respectively. We define the "distance" between the two particles using their transverse momenta $\mathbf{k_t}_i$ and $\mathbf{k_t}_j$ in the following way:

$$d_{ij} = min\left(\frac{1}{\mathbf{k_t}_i^2}, \frac{1}{\mathbf{k_t}_j^2}\right)\frac{\Delta R_{ij}^2}{R^2} \tag{2.2}$$

where ΔR_{ij} is the separation in the (η, ϕ) plane and R is a parameter which stands for the radius of the cone. In addition to the separation between the particles d_{ij}, the separation between a single particle and the beam d_{iB} is also defined:

$$d_{iB} = \mathbf{k_t}_i^2 \tag{2.3}$$

The clustering algorithm consists in selecting two particle and evaluating if they can be combined together according to which is greater between d_{ij} and d_{iB}. After this, the procedure is repeated until no free particle remains. The general behaviour of the clustering algorithm can be explained relating to distance ΔR_{ij}. If, for example, there is a hard particle surrounded by many soft particles in a region of $2R$, the soft particles will cluster around the hard one, and not between them. When there are two near hard particles, if $R < \Delta_{ij} < 2R$ then the two particles are considered as two separated jets. If, though, $\Delta_{ij} < R$, they are clustered together. The main advantage of this method is that the soft particles does not modify too much the shape of the jet, which is mainly due to the hard ones.

The jet reconstruction and the detector simulation is performed by *Delphes 3* [50]. Delphes is a C++ framework for fast performing multipurpose detector simulations. It is interfaced with the file formats we have as output of the previous steps simulation and return observables such as isolated leptons, missing transverse energy ($\not{E}_T$) and jets. The output is given in the ROOT ntuple format. The detailed description of the output of Delphes can be found in [51]. At this point, we have to choose the card corresponding to the simulator of our experiment. In our case we select the CMS card, which contains the parameters, such as the efficiency of the tracker and the calorimeters.

Now the procedure for the complete simulation is ready. With the proper settings we are able to perform the simulation of the Dark Matter EFT signal according to our model and of the neutrino background originated by the Z^0 and W decays from the parton-level scattering to the detector response. In the following sections of the chapter the method used to select the mono-jet events from all of the events generated will be

discussed. The method to implement the additional cut on the center of mass energy E_{CM} is also explained because it will be necessary to test the theoretical range of validity of our EFT model (M_{cut}).

2.2 Signal and Background Simulation

First of all, we will discuss the simulation of the Dark Matter signal predicted by our Effective Field Theory model, namely how we can translate the physics we discussed in an input for our simulation chain.
We performed seven simulation of our Dark Matter signal, one for each m_{DM} we choose to test. The chosen masses are displayed in the following table:

Mass [GeV]						
1	100	200	400	600	800	1000

As it was said in the first chapter, we are searching Dark Matter in the form of Weakly Interacting Massive Particle (WIMP). Under this assumption, we have to consider the possibility that these particles have a mass in the range of GeV-TeV. We chose the mass values as a consequence of this hypothesis.

Once the model is implemented with FEYNRULES and loaded in *MG*5, we have to specify the details of the processes we want to generate. We obviously must set the particles involved first. We suppose that the most probable processes that can generate a mono-jet event in the detector are the following:

- $pp \to xx$
- $pp \to xxj$
- $pp \to xxjj$

where x is the DM particle, "p" is the multiparticle set representing a proton. With" p" we mean a set including up, down, strange quarks and antiquarks and gluons because, as it was said before, the proton is not a fundamental particle, but it has an internal structure. With the label "j" we mean "light jet", namely a multiparticle including quarks, antiquarks and gluons in the final state which, after the showering and hadronization process, can create a QCD jet in the calorimeter of the detector. With this instructions, we want *MG5* to allow MADEVENT to generate a sample in which each event could be one of these three, according to their probability (square module of the matrix element).

The figure 2.1 shows two examples of hard-scattering processes MG5 generates belonging to the $pp \to xxj$ category. The three kinds of process listed above have different matrix elements and they populate different regions of the parameters space. After the mono-jet event selection is performed, we will notice that the surviving events will be mainly composed by the second type, which is the target of the cuts.

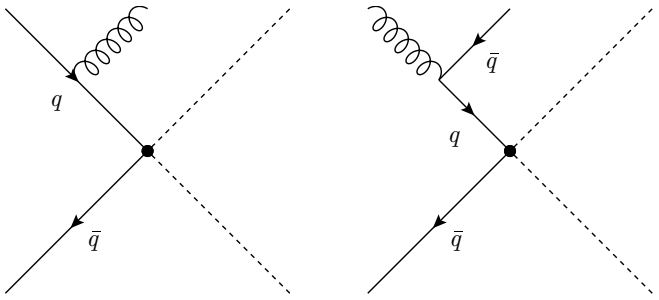

Figure 2.1: The two panels show the Feynman diagrams of two possible dark matter creation processes. The presence of an extra-parton is required to reproduce the mono-jet event category.

The parameters of the phase space of the simulation must be set. This can be done by modify the *runcard.dat* in the folder of the simulation. First of all we have to specify the number of parton-level events we want to generate N_{pl} and the center of mass energy of the proton-proton collisions E_{CM}.

N_{pl}	E_{CM}
1'000'000	13

E_{CM} is expressed in TeV. The MLM matching scheme is selected by setting to "1" the *ickkw* parameter. Moreover, we need to set the parameters in (2.1).

p_T^{min}	η^{max}	R^{min}
30	7	0

p_T^{min} is expressed in GeV. R_{min} is automatically set to zero when we set $p_T^{min} > 0$. The last one important parameter to set at this point of the simulation is the maximum number of quark flavours than can appear in the final state of the parton level process. Given that the center of mass energy is 13 TeV, we assume to be possible to have a *bottom* quark in the final state, so the maximun number of quarks flavour is five (the top quark is always rejected in these kind of processes because it is to heavy). Now we have to set the Pythia parameters for the matching and for the parton shower/hadronization (modifying the *pythiacard.dat*). We select a p_T-ordered shower by setting the parameter *MSTP(81)* larger than 20. The parton shower and the hadronization are switched on by setting $MSTP(61) = 1$ and $MSTJ(1) = 1$ respectively. The main physical parameter in Pythia setting is the cut-off on the transverse momentum of the shower jet Q_{cut}, which is set to 100 GeV. Q_{cut} must be larger than p_T^{min} of MADEVENT for consistency. For the detector simulation, all we need to set in Delphes is contained in the default CMS card. The only things we modify is the selection of the anti-k_t algorithm for the jet reconstruction in the CMS card.

As concerns the background simulation, the setting of the three softwares are exactly the same because we want to obtain a result which is consistent with the signal simulation. The main difference is, of course, the hard scattering processes involved. As we explained in the first chapter, the standard model processes with the same footprint of our dark matter signal are those involving neutrinos production. We have two sources of neutrinos, which are the decay of the Z^0 and of the W bosons. As input of MG5, we use a syntax similar to the Dark Matter case. For the simulation of the Z^0 decay we set:

- $pp \to \nu\nu$
- $pp \to \nu\nu j$
- $pp \to \nu\nu jj$

where ν is a multiparticle set standing for all leptonic flavours neutrinos and anti-neutrinos. For the W decay we have:

- $pp \to \nu l$
- $pp \to \nu l j$
- $pp \to \nu l jj$

where ν now means neutrinos and anti-neutrinos, and l stands for all leptons and anti-leptons. For the background, in addition to the settings previously discussed in section 1.3.2, we implemented other "generation level" cuts, namely some conditions for the event to be generated at parton-level. These conditions regards the transverse momentum of the mediator bosons.

$p_T^{min}(Z^0)$	$p_T^{min}(W)$
150	130

The values of $p_T^{min}(Z^0)$ and $p_T^{min}(W)$ are expressed in GeV. The reason why we use the generation-level cuts is that the mono-jet efficiency on these processes is high, so only a few events would survive the selection. To solve this problem we can simulate a sample more than ten times bigger than before, but this will lead to long-time simulations, so we decided to implement the additional cuts to obtain parton-level events which already belong to the region of interest in the parameter space.

In addition to the information about the observables of the events, MG5 gives us also the cross section value σ_{MG} of the complete simulation (MG5+Pythia+Delphes). In the signal simulation, besides the value of the Dark Matter mass, we set a reference value of the energy scale of the theory M_*, define in 1.1.1, of 1 TeV. This will lead to a reference cross section value for each simulation. The values of the reference cross section $\bar{\sigma}(M_* = 1TeV)$ of the different dark matter mass simulations are displayed in the following table.

Mass [GeV]	1	100	200	400	600	800	1000
$\bar{\sigma}$ **[pb]**	24.54	16.09	10.71	5.12	2.57	1.32	0.68

This reference cross sections will be useful for the parameterization of the true signal cross section, in which the dependence on M_* will be made explicit. As we will see in the following section, with the mono-jet event selection the actual cross section we will use for the analysis will be nearly a hundred times lower. This is due to the efficiency of the selection. The events of this process are distributed in $\not{E}_T$ approximately as a power-law ($\sim t^{-\alpha}$) and this means that the majority of the events will take place in the low-$\not{E}_T$ region. Placing a lower cut-off on the $\not{E}_T$ value would mean rejecting most of the events.

2.3 CMS MONO-JET EVENT SELECTION

After the complete simulation procedure we obtain a file, in the format of a ROOT ntuple, containing all the information about the generated events such the $\not{E}_T$ or the $\mathbf{p_T}$ o f the jets. From this list of events coming out of the simulation chain, we need to select the ones which have the characteristics to be considered *mono-jet* events. A mono-jet event, as we said in 1.3.2, is an event characterized by one high transverse momentum jet and a high value of $\not{E}_T$ seen as the recoil of the jet. As we said, this kind of event is suitable for our dark matter signal because in our EFT model the hard jet can be originated by a parton emission and the $\not{E}_T$ recoil can be seen as the transverse momentum of the couple of dark matter particles. The selection is carried out by implementing the cuts described in the previous chapter.

For the analysis of the ROOT ntuples we used the pyROOT environment. The cuts were implemented this way: after selecting event per event the variables involved, such as the transverse momentum of a jet or its pseudo-rapidity, and the cuts are imposed as a sequence of *if* conditions. At the end, we obtain the subsample of the mono-jet events. The most important information we need from the event selection is the efficiency of the cuts. To obtain a consistent parameterization of the cross section predicted by our EFT, we need to know how much the number of events is reduced when we place some cuts on the parameter space. The efficiency will depend on the value of the dark matter mass and, of course, on the value of M_{cut}, whose implementation will be discussed later in this section. In 2.2 the $\not{E}_T$ distribution and the cut efficiencies are displayed for the simulation of a 200 GeV Dark Matter (we suppose an integrated luminosity of 2.24 fb^{-1}) .

As we can see from the efficiencies figure in 2.2 the mono-jet selection total efficiency is around 3 per cent, as we expect. The strongest cut is the jet-p_T one combined with the minimun $\not{E}_T$.

We implemented the same type of cuts for the background simulation,but we need an additional condition for the W-background. In this type of event, the neutrino is

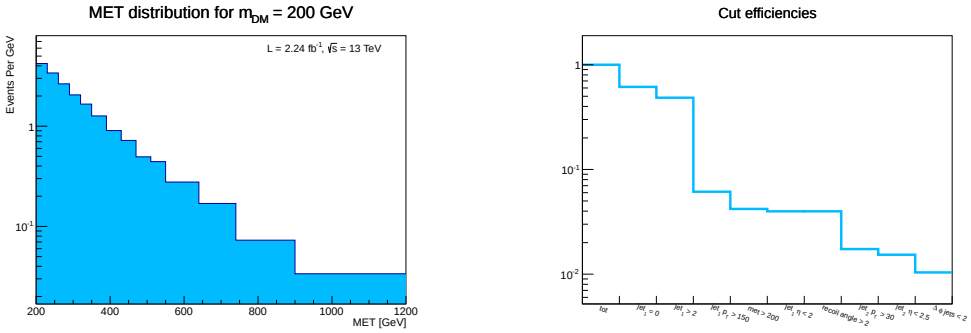

Figure 2.2: In the left panel the $\not{E}_T$ distribution of our dark matter signal is displayed for a given mass of 200 GeV. In the right panel we show the efficiencies of the single cuts in the mono-jet selection. The ratio between the bins' values gives the exact efficiency for each cut.

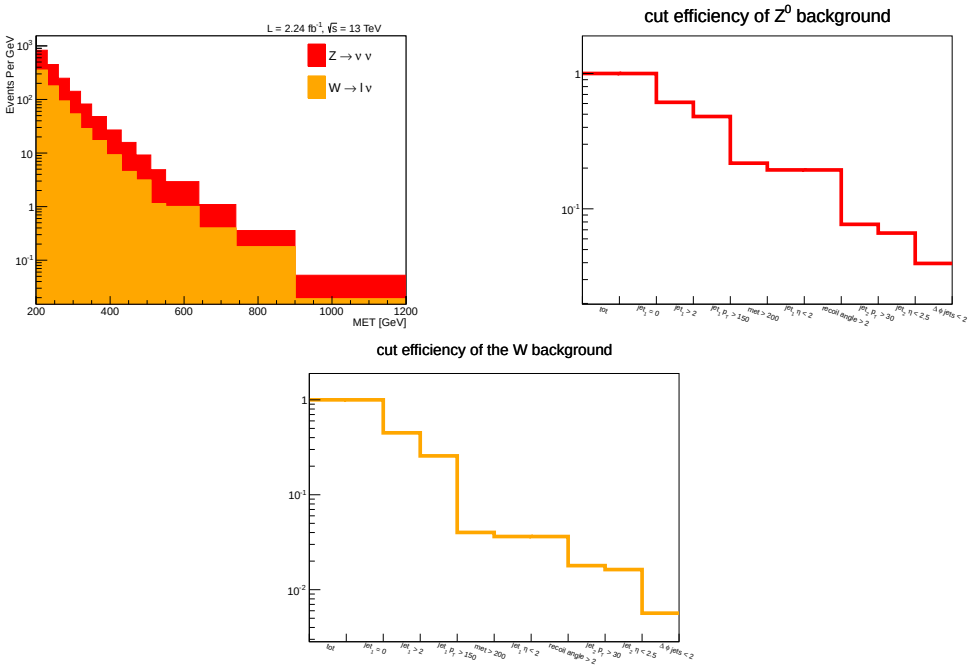

Figure 2.3: In the figures above the total neutrino background $\not{E}_T$ distribution and the efficiencies are displayed.

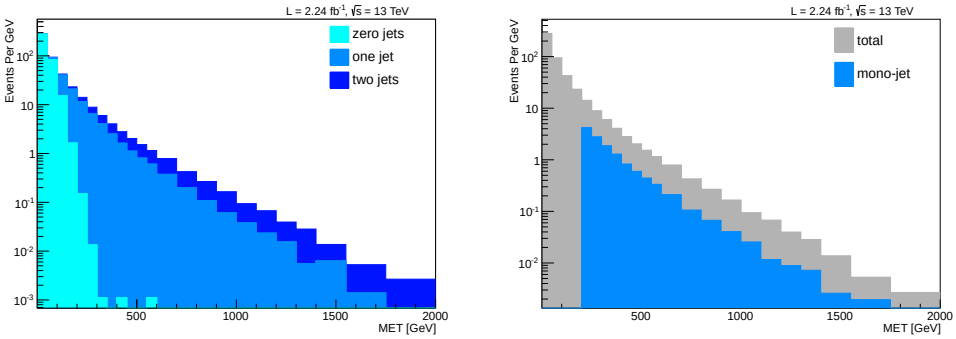

Figure 2.4: The figures above show $\not{E}_T$ distribution of the $m_{DM} = 200$ GeV events simulation. In the left panel the events are divided depending on the number of extra partons in the hard scattering. The right panel shows the $\not{E}_T$ distribution after the mono-jet selection compared with the total event distribution.

produced simultaneously with a lepton so, if the detector can see this lepton, the event can be tagged as W-decay and reject from the mono-jet + $\not{E}_T$ category. So, in the cut implementation for the background, we additionally impose the lepton to be *slow* or *forward*, namely $p_T^{lepton} < 10$ GeV or $\eta^{lepton} > 2.4$. In either these two situations, the lepton could not be seen by the detector and so the event is tagged as mono-jet. In 2.3 the $\not{E}_T$ distribution of the total background and the efficiencies are displayed supposing an integrated luminosity of 2.24 fb^{-1}. Regarding the efficiencies, we have to take into account that, in the simulations of both kinds of backgrounds (Z^0 and W), a pre-cut on the transverse momentum was performed inside the simulation process. So, as we can see from 2.3, the offline cut on the $\mathbf{p_T}$ of the final state particles is less efficient respect to dark matter case. If we would have considered a background simulation without the pre-cuts, the total efficiency of the offline cuts would have been much more higher.

The total efficiency for the background simulation is shown in the following table:

	$\mathbf{Z^0}$	**W**	**total**
Efficiency	0.1262	0.0103	0.0278

In fig. 2.4 we can see some effects of the mono-jet event selection. The left panel shows the composition of the $\not{E}_T$ distribution of the signal before the implementation of the selection. We can notice that most the events are generated without any extra parton and they populate mainly the low $\not{E}_T$ region. Unfortunately, this kind of events is undetectable, as we said in the previous chapter. The reason they populate the low $\not{E}_T$ region is that without an extra parton, the two dark matter particles go to opposite directions when they are produced because of the total transverse momentum conservation. As a consequence, the total $\not{E}_T$ of the event is zero. In the right panel the

actual mono-jet $\not{E}_T$ event distribution and the total one are displayed. Comparing the to images, we can notice that the of the off-line cuts isolate the events with only one extra parton at generation level.

The CMS cuts are compulsory if we want to isolate the mono-jet events for the statistical analysis. In the next section, we will discus another kind of offline cut, the cut on the E_{CM} of the process.

2.3.1 Invariant Mass Cut

In the first chapter, when the EFT model was discussed, we defined the parameter M_{cut}, which represents the scale of validity of our theory, as we said in section 1.1.1. This is a bound on the center of mass energy of the event E_{CM}, namely our EFT gives good prediction only for processes with $E_{CM} < M_{cut}$. In order to test different values of M_{cut} we need to implement a cut similar to what we did in the previous section. The problem with the M_{cut} implementation is that we cannot know the exact center of mass energy E_{CM} of the parton-level process from the observables measured by the detector. This is due to the fact that LHC performs proton-proton collisions. We know that the E_{CM} of the the two protons is 13 TeV, but the fundamental process is the one between partons, each one carrying an unknown fraction of the total momentum of the proton.

So the cut on E_{CM} must be considered separately from the other. We need to know the momentum of the outgoing partons in the fundamental process in order to implement it. These values can be obtained from information we have about the parton level simulation. Considering that from the real experiment at LHC we would not know this, we say that it is a *theoretical cut*. The E_{CM} of a process is calculated by squaring the total 4-momentum of the final state particles. To obtain the total 4-momentum we obviously need to know the contribution of the two outgoing dark matter particles (that we can not measure with the detector).

We decided to implement and test three methods to evaluate E_{CM} for each event.

1. **Leading jet** : the total 4-momentum of the process is obtained summing the 4-momentum of the two outgoing dark matter particle and of the $\mathbf{p_T}$-leading jet after the jet reconstruction. The value of E_{CM} is the squared total 4-momentum.

2. **Multiple jets** : the jets of an event are selected and ordered in p_T. Then the leading jet's 4-momentum is summed to the one of the dark matter particles. If the transverse component of the total 4-momentum calculated this way is at least the 90 percent of the event's $\not{E}_T$, E_{CM} is calculated squaring the total 4-momentum. If this does not happen, the second p_T-ordered jet is considered, its 4-momentum is summed to the previous one and then the transverse component is evaluated again. The procedure goes on until the $\not{E}_T$ value is balanced at 90 percent by the jets.

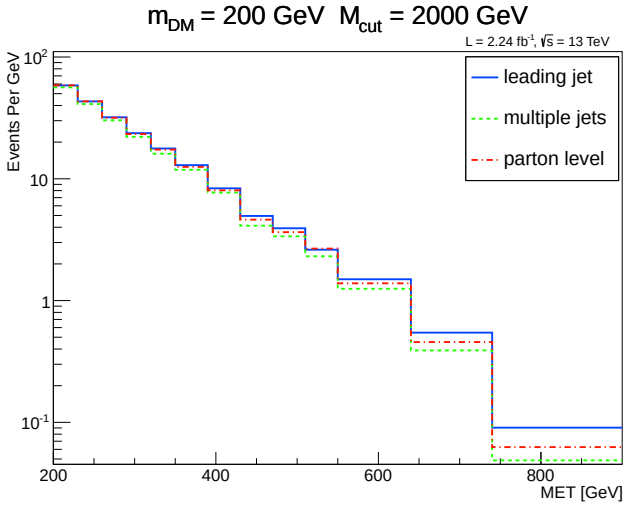

Figure 2.5: E_{CM} calculation methods comparison

3. **Parton level invariant mass** : the 4-momentum of all the outgoing particles (dark matter and light partons) of the event is summed and squared to obtain E_{CM}. The main difference of this method respect to the others is that is fully based on the parton-level process.

The third method is the most accurate because the result is the true value of E_{CM} without approximations (as in the other two cases), but the fact that is not related with any of the observables of the detector may lead to a consistency problem.
We decided to test all the three methods and to verify the agreement. The parton-level method will be chosen if it gives a good agreement with the other two methods.
In figure 2.5 the $\not{E}_T$ distribution is plotted for $m_{DM} = 200$ GeV and $M_{cut} = 2000$ GeV. As we can see, the three methods give very similar results, so the parton-level method is chosen for further analysis.

Once the method to calculate E_{CM} for each event is established, the cut-off is imposed as an *if* condition in the algorithm. If $E_{CM} > M_{cut}$, the event is rejected. From each dark matter EFT signal simulation we can obtain a set of samples with different M_{cut} values. We decided to use seven different values of M_{cut}. The highest value is the so called *Naive EFT*, namely when no cut on the center of mass energy is imposed. Of course, this is equivalent to setting $M_{cut} = 13TeV$, which is the maximum range of LHC. The values of M_{cut} are displayed in the following table:

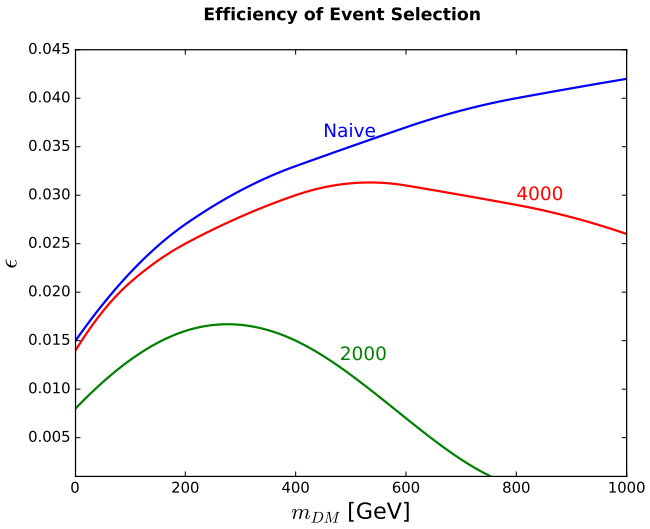

Figure 2.6: The figure shows the behaviour of the efficiency ϵ depending on the dark matter mass m_{DM} and M_{cut}.

$\mathbf{M_{cut}}$ [GeV]						
500	750	1000	1500	2000	4000	13000

In order to have an explicit expression for our parameters, we need to parameterize consistently the cross section of our EFT signal σ_{EFT} in the signal region. Our starting point is of course the results of the Monte Carlo simulations. We will use the reference cross sections obtained with the simulations and we need to take account the fact the we are counting events in a well determined region of the possible phase space. As we said before, this region depends on the CMS mono-jet selection cuts and on the E_{CM} cut. The efficiency ϵ will appear as a multiplicative factor in the expression of σ_{EFT}.

It is interesting to study the dependence of the efficiency on the parameters of the simulation, namely m_{DM} and M_{cut}. Figure 2.6 shows the behaviour of the efficiency $\epsilon(m_{DM}, M_{cut})$. As we can see, the value of ϵ increases when m_{DM} increases, this means that events with heavier dark matter are enhanced in the mono-jet selection. For values of M_{cut} different from ∞, we notice that at a certain mass value the efficiency start to decrease and even goes to zero. The reason is that placing a upper limit on the center of mass energy of the process reduces the energy budget of the reaction, so dark matter particle that are heavier than a certain threshold can not be produced. The low number of events when m_{DM} approaches the threshold deteriorates and even kill the signal in acceptance. This threshold is given by:

$$m_{DM}^{max} = \frac{M_{cut}}{2}\sqrt{1 - 2\frac{\not{E}_T}{M_{cut}}} \tag{2.4}$$

The efficiency can also depend on the signal region selection, as we will see in the following chapter. The concept does not change, the efficiency calculation is necessary to rescale the total reference cross section to the region isolated with the cuts.

Hence, we decide to parameterize the total EFT cross section as follows:

$$\sigma_{EFT}(M_*, m_{DM}, M_{cut}) = \left[\frac{1TeV}{M_*}\right]^4 \cdot \bar{\sigma}(m_{DM}) \cdot \epsilon(m_{DM}, M_{cut}) \tag{2.5}$$

As we can see, we have and explicit dependence on the energy scale of the theory M_*, which appears as a factor $\frac{1}{M_*^4}$. This is consistent with our EFT model. As we said in the first chapter, our EFT model consists in integrating out the degrees of freedom related to the mediator and thus obtaining an approximated theory. The coupling strength of the operator is proportional to $\frac{1}{M_*^2}$ and, as a consequence, the cross section will be proportional to its squared value. The explicit dependence on M_* is fundamental for the limit setting strategies because it will allow us to set a lower bound on it for each combination of m_{DM} and M_{cut}.

As we explained in sect. 1.1.1, the invariant mass cut-off M_{cut} is a fundamental parameter for the description of an EFT because it determines the range of validity of our approximation. Assuming that we can consider as independent the events with different centre of mass energy E_{CM}, once M_{cut} is fixed, we can divide the signal into two subsets. The first includes the events with $E_{CM} < M_{cut}$, namely the events predicted by the EFT, while the second includes all the other events with $E_{CM} > M_{cut}$ whose behaviour will depend on the underlying UV theory. Therefore, we can say that the number of events predicted by the EFT approximation (or alternatively the cross section) underestimates systematically the true value of the signal, namely:

$$\sigma_{EFT} \leq \sigma_{true} \tag{2.6}$$

The above consideration is fundamental in the limit setting strategy presented in the next chapter because allows to set a limit on the parameters of the effective theory.

CHAPTER 3

STATISTICAL ANALYSIS

Our EFT dark matter model is characterized by three parameters, the energy scale of the theory M_*, which appears in the coupling strength of the interaction as a factor $1/M_*^2$, the mass of the dark matter particles m_{DM} and the EFT cut-off M_{cut}. The EFT does not provide, strictly speaking, a prediction for the signal. It only predicts lower bounds on the signal, which however are enough to set limits on the EFT parameters. The strategy we decided to adopt consists in setting a bound on the parameter M_* in function of m_{DM} and M_{cut}. For fixed values of m_{DM} and M_{cut}, we evaluate the lowest possible value of the parameter M_* in a determined kinematical region, based on the condition that the signal predicted must be lower than the maximum value of extra signal we can obtain in that region, according to the background values.

In the next sections two different statistical procedures to set the lower bound on M_* will be explained.

3.1 CUT AND COUNT

The first one is the so called *Cut and Count* method. It consist in selecting a suitable *signal region* and focus the analysis only on the signal and background events belonging to that region. These regions are selected by setting a lower cut-off on the $\not{E}_T$ of the event $\not{E}_T^{min}$, namely we consider part of the signal region the events with $\not{E}_T > \not{E}_T^{min}$. The signal region selection will affect the parameterization of the EFT cross section, namely the efficiency ϵ will be modified by the restriction of the signal region due to the lower cut on the $\not{E}_T$. The cross section parameterization in 2.5 takes the form:

$$\sigma_{SR}(M_*, m_{DM}, M_{cut}, \not{E}_T^{min}) = \left[\frac{1TeV}{M_*}\right]^4 \cdot \bar{\sigma}(m_{DM}) \cdot \epsilon(m_{DM}, M_{cut}, \not{E}_T^{min}) \qquad (3.1)$$

The choice of the optimal signal region will depend on the parameters M_{cut} and m_{DM}.

For each value of M_{cut} the proper signal region will be chosen to give the best bound possible.

3.1.1 Hypothesis test, a simplified example

To set limits we will use the a procedure called *Hypothesis Test*. An hypothesis test is a procedure used to discriminate if a model (the hypothesis) is compatible with the data set of an experiment. A more detailed description can be found in [52–54]. The first step is defining the model. With the word model we mean a probability density function (p.d.f.) we suppose to be the distribution of our data sample. This p.d.f. will depend on some unknown parameters we want to determine from the data set we have at our disposal.

To perform the hypothesis test we need to define a variable, the *test statistic*, depending both on the parameters and on the data, which discriminates whether our model fits the data or not with a fixed probability (*confidence level*). We need to set a limit on our parameter, so we will impose a certain confidence level (95 %), we will calculate the corresponding value of the test statistic and from it we extract the value of our lower limit on M_* according to the given C.L. .

Now we will describe the procedure for our model. We will explain a simplified version first, in order to test the behaviour of our data and to understand properly the procedure. The complete method will be discussed in the next section. The starting point is the number of observed data $\mathcal{O}$, which will be our random variable. We suppose to have a sample of mono-jet events detected by CMS. From these, we select a subsample determinate by their value of missing transverse energy, namely we select the events that have $\not{E}_T > \not{E}_T^{min}$. We suppose $\mathcal{O}$ to have a Poisson distribution around an expected value given by the sum of the background and the signal $B + S$. In this simplified version, we suppose to know the B value without uncertainty.

The p.d.f. of the sample will be:

$$f(\mathcal{O}|B+S) = \frac{(B+S)^{\mathcal{O}}}{\mathcal{O}!} e^{-(B+S)}$$

If the value of $\mathcal{O}$ is sufficiently large, we can approximate the Poisson distribution with a Normal with expected value $B + S$ and standard deviation $\sqrt{B+S}$. The p.d.f. thus will be:

$$f(\mathcal{O}|B+S) = \frac{1}{\sqrt{2\pi(B+S)}} e^{-\frac{1}{2}\frac{(\mathcal{O}-(B+S))^2}{B+S}}$$

In our case, instead of the p.d.f., we are interested in the *likelihood* associated to our hypothesis. The likelihood has the same form of the p.d.f. seen as a function of the parameters instead of the data. The likelihood will be defined as follows:

$$\mathcal{L}(B+S) = f(\mathcal{O}|B+S) = \frac{1}{\sqrt{2\pi(B+S)}} e^{-\frac{1}{2}\frac{(\mathcal{O}-(B+S))^2}{B+S}} \tag{3.2}$$

The Bayesian interpretation of *likelihood* is the probability of a hypothesis to be true given the data sample. It depends then on the value of the parameters we suppose. Now that we have defined a proper likelihood function for our system, we can build our test statistic. We start defining the likelihood ratio λ as the ratio between 3.2 and its maximum, obtained for $B+S=\mathcal{O}$

$$\lambda(B+S) = \frac{\mathcal{L}(B+S)}{max(\mathcal{L})} = e^{-\frac{1}{2}\frac{(\mathcal{O}-(B+S))^2}{B+S}}; \tag{3.3}$$

From the likelihood ratio λ we can extract the χ^2 variable, which we will use as test statistic, defined as follows:

$$\chi^2 = -2\log(\lambda) = \frac{(\mathcal{O}-(B+S))^2}{B+S} \tag{3.4}$$

It can be shown (see [54]) that if the value of $B+S$ is sufficiently large so that if the observed $\mathcal{O}$ can be treated as gaussian, our variable χ^2 will follow a χ^2 p.d.f. . In our case, the number of degrees of freedom of the χ^2 p.d.f. is 1, because we have only a free parameter to evaluate. If we want to obtain a confidence interval of 95 percent on the signal S we have to impose the *p-value* of our hypothesis to be lower than 5%, namely $p < 0.050$. The p-value of an hypothesis is a quantity, computed *a posteriori*, which stands for the probability, given the data, to obtain a better agreement with the data repeating the experiment. The p-value is used to test the agreement between an hypothesis and the data. The lower is its value, the better the hypothesis agrees with the data sample. In our case we impose:

$$p = \int_{\chi^2_{obs}}^{\infty} f_{\chi^2}(\chi^2) d\chi^2 < 0.050 \tag{3.5}$$

In therms of our χ^2 variable this means:

$$\chi^2_{obs} = \frac{(\mathcal{O}-(B+S))^2}{B+S} < 3.84 \simeq 4 \tag{3.6}$$

Solving this equation is the way to find the 95% confidence level interval on the signal S given the value of the background B and the observed $\mathcal{O}$. At this point, the *background-only* condition ($\mathcal{O}=B$) can be imposed. This hypothesis is based on the assumption that no relevant event excess will be observed by the CMS detector. Therefore, all the observed events will belong to the standard model background. We obtain an approximated equation for S:

$$\frac{S^2}{B+S} < 4 \tag{3.7}$$

The solution of eq. (3.7) gives us the maximum value the signal S can have given the background and its statistical fluctuations. The result is:

$$S_{max} = 2 + 2\sqrt{1+B} \simeq 2\sqrt{B} \tag{3.8}$$

the approximation in the above result is consistent because we supposed that $B \gg 1$ for the gaussian approximation in 3.10. At this point, the maximum cross section allowed σ_{exc} is easily calculated dividing S_{max} by the integrated luminosity L of the experiment. As we can see, the value of σ_{exc} depends on the background value which depends itself from the region in $\not{E}_T$ we chose. So, σ_{exc} depends on the minimum value of $\not{E}_T$ we used to select the signal region. Hence, the value of the lower bound on M_* will depend on σ_{exc} and as a consequence the minimum of $\not{E}_T$ will be set to obtain the greater value of M_*^{exc}. In the following sections the complete hypothesis test and the procedure to get the M_*^{exc} value will be explained.

3.1.2 Hypothesis test in presence of nuisance parameters

Now we will explain the full procedure we decided to adopt for the Cut and Count analysis. It is very similar to the simplified one, but now we will consider the error on the background value. The error will be treated as a *nuisance* parameter [52]. The likelihood of a given hypothesis could depend on parameters we are not directly interested in measuring, the so called *nuisance* parameters. The lack of information about those parameters affects the accuracy by which the parameters of interest can be determined.

The method commonly used to treat the nuisance parameters is the *profile likelihood ratio* [52–54]. It is an approximation that consists in finding the curve in the parameter space where the likelihood ratio is maximum with respect to the nuisance parameters. The result obtained can be treated as the χ^2 variable in the previous case.

In addition to the distribution of the observed data $\mathcal{O}$, in this case we suppose to know also the distribution of a nuisance parameter ν corresponding to the uncertainty on the background value. We parameterize the background B as follows.

$$B = \bar{B} \pm \delta B = \bar{B} \pm \epsilon \bar{B} = \bar{B} \cdot (\epsilon \pm 1) = \nu \bar{B} \tag{3.9}$$

ν is a parameter which represents the uncertainty on the background. It has a mean value of 1 and a standard deviation $\delta\nu \ll 1$. We suppose ν to have a Normal distribution:

$$f_\nu(\nu, \delta\nu) = \frac{1}{\sqrt{2\pi}\delta\nu} e^{-\frac{1}{2}\frac{(\nu-1)^2}{\delta\nu^2}}$$

The observed $\mathcal{O}$ is distributed as in the previous case, with B parameterized as in 3.9.

$$f(\mathcal{O}|\nu\bar{B} + S) = \frac{1}{\sqrt{2\pi(\nu\bar{B} + S)}} e^{-\frac{1}{2}\frac{(\mathcal{O}-(\nu\bar{B}+S))^2}{\nu\bar{B}+S}}$$

If we suppose that $\mathcal{O}$ and ν are independent random variables, the likelihood is the joint p.d.f., namely:

$$\mathcal{L}(S, \nu) = \frac{1}{2\pi\sqrt{(\nu\bar{B} + S)}\delta\nu} e^{-\frac{1}{2}\frac{(\mathcal{O}-(\nu\bar{B}+S))^2}{\nu\bar{B}+S}} e^{-\frac{1}{2}\frac{(\nu-1)^2}{\delta\nu^2}} \tag{3.10}$$

Before computing the profile likelihood ratio, we make an approximation to simplify our calculation. The factor $e^{-\frac{1}{2}\frac{(\nu-1)^2}{\delta\nu^2}}$ is nearly zero when the value of ν is too different from 1, so we can put $\nu\bar{B} + S \simeq \bar{B}$ except in the factor $(\mathcal{O} - (\nu\bar{B} + S))^2$, where it plays a fundamental role.

The approximated total likelihood takes the form:

$$\mathcal{L}(S, \nu) \simeq \frac{1}{2\pi\sqrt{(\bar{B} + S)}\delta\nu} e^{-\frac{1}{2}\frac{(\mathcal{O}-(\nu\bar{B}+S))^2}{\bar{B}+S}} e^{-\frac{1}{2}\frac{(\nu-1)^2}{\delta\nu^2}} \tag{3.11}$$

Now we can compute the profile likelihood ratio:

$$\lambda_p = \frac{\mathcal{L}(\hat{\hat{\nu}}(S), S)}{max(\mathcal{L}(\nu, S))} \tag{3.12}$$

where $\mathcal{L}(\hat{\hat{\nu}}(S), S)$ is the likelihood maximized for ν keeping S fixed and $max(\mathcal{L}(\nu, S))$ is the maximum value of the likelihood. Finding the maximum value for the likelihood is equivalent to find the minimum value of its exponent. The expression of the maximized likelihood is:

$$\mathcal{L}(\hat{\hat{\nu}}(S), S) = \frac{1}{2\pi\sqrt{(\bar{B} + S)}\delta\nu} e^{-\frac{1}{2}\frac{(\mathcal{O}-(\bar{B}+S))^2}{\delta\nu^2\bar{B}^2+\bar{B}+S}}$$

and as a consequence the profile likelihood ratio is

$$\lambda_p(S) = e^{-\frac{1}{2}\frac{(\mathcal{O}-(\bar{B}+S))^2}{\delta\nu^2\bar{B}^2+\bar{B}+S}} \tag{3.13}$$

Now we can proceed as in the previous case. The χ^2-variable is now

$$\chi^2 = -2\log(\lambda_p) = \frac{(\mathcal{O} - (\bar{B} + S))^2}{\delta\nu^2\bar{B}^2 + \bar{B} + S}$$

After imposing the background-only condition and solving the corresponding equation for a χ^2 with 1 degree of freedom, we obtain our new maximum signal allowed:

$$S_{max} = 2 + 2\sqrt{1 + \bar{B} + \delta\nu^2\bar{B}^2} \simeq 2\sqrt{\bar{B} + \delta\nu^2\bar{B}^2} \tag{3.14}$$

The maximum cross section allowed σ_{exc} is calculated the same way as in the previous case. Introducing the background error will deteriorate the bound on M_*. The uncertainty of the background reduces the accuracy of the data we have at our disposal and therefore the value of S_{max} increases. As we will see in the next section, a higher value of S_{max}, and consequently of σ_{exc}, will reduce the lower bound M_*^{exc}.

Now that we have a way to calculate the maximum cross section allowed σ_{exc} we can proceed with the lower bound M_*^{exc} setting. In the next section we will define the method to select the best signal region and how the value of M_*^{exc} is calculated.

3.1.3 Limit Setting

Once m_{DM}, M_{cut} and t_0 are fixed, we can compute the value of M_*^{exc} by using the property that the signal predicted by our EFT systematically underestimate the true value, namely the value that we would obtain if we knew the complete model.

The equation can be obtained by imposing this condition:

$$\sigma_{EFT} \leq \sigma_{exc} \Rightarrow \left[\frac{1TeV}{M_*}\right]^4 \cdot \bar{\sigma}(m_{DM}, M_{cut}) \cdot \epsilon(m_{DM}, M_{cut}, \not{E}_T^{min}) \leq \sigma_{exc}$$

and, as a consequence, the expression for M_*^{exc} is:

$$M_* \geq M_*^{exc} = \sqrt[4]{\frac{\bar{\sigma} \cdot \epsilon}{\sigma_{exc}}} \tag{3.15}$$

As we can see, it depends on the dark matter mass, on M_{cut} and on the $\not{E}_T$ signal region cut $\not{E}_T^{min}$. We can use the dependence on t_0 to select the optimal signal region for the bound calculation. The procedure of signal region selection consists in calculating the value of M_*^{exc} modifying the cut-off on the Missed Transverse Energy until the maximum value of the lower bound is obtained. For each value of M_{cut} we will obtain a corresponding value of the optimal t_0. Once M_{cut} and t_0 are fixed, the calculation of M_*^{exc} is performed for each m_{DM} value. As a result, we will obtain a curve in the (M_*^{exc}/m_{DM}) plane for each M_{cut} value.

The Cut and Count method provides us a good conservative lower bound on M_*, but it ignores all the data outside the cut and count region, while these data could be significant to improve signal rejection. In the next section we will discuss a new procedure based on the same EFT property of underestimation, but able to take into account all the information we have from our data to obtain a better conservative lower bound on M_*.

3.2 Modified Shape Analysis

A *Shape Analysis* is a procedure to define a likelihood function for a system taking into account its distribution along a given variable. For example, we can suppose to divide the signal events of a given process in n different bins of an observable t. For each bin we have the number of signal events S_i. In order to be effective, the shape procedure requires the bins to be correlated by at least one parameter, which is the same for each bin. To do so, we can parameterize the signals as follows

$$S_i = \mu \cdot s_i \tag{3.16}$$

where μ, the so called *signal strenght*, is the same for each bin, while the bin-dependence is given by s_i. At this point, the likelihood of the system can be defined as the product of the single-bin likelihoods and it can be used for the analysis. Moreover, if the events in each bin follow a Normal distribution, a total-χ^2 variable can be defined similarly to 3.4 and it will follow a χ^2-distribution with n degrees of freedom.

However, we cannot use this procedure for our EFT signal, because it does not account for the true signal distribution, but only for the events with $E_{CM} < M_{cut}$. In the case of EFT analysis we would have

$$S_i^{true} \geq S_i^{EFT} = \mu \cdot s_i^{EFT} \tag{3.17}$$

To overcome this problem, in the next section we will introduce a *Modified Shape Analysis*, based on a signal parameterization of the kind

$$S_i^{true} = \mu \cdot s_i^{EFT} + \Delta S_i \tag{3.18}$$

where $\Delta S_i \geq 0$ accounts for the signal not predicted by the EFT.

3.2.1 Shape Analysis Procedure

In this section we will discuss the procedure we introduce to calculate the bounds on the parameters of the theory. Suppose to divide our simulated signal and background in "n" bins of $\not{E}_T$, each bin is labelled with the index $i = 1...n$. For each bin we define our random variable $\mathcal{O}_i$, corresponding to the number of events observed in the "i"-th bin, as in the previous case. We also define the expected value $E_i = B_i + S_i + \Delta S_i$, where:

- $\mathbf{B}_i$ is the expected value of the background in the bin. As in the previous case, we will also introduce the error on the background $\delta\nu_i$ parameterizing $B_i = \nu_i \bar{B}_i$. The error will be treated as before in each bin.

- $\mathbf{S}_i$ is the EFT predicted signal in the bin. The value of S_i is parameterized similarly to the Cut and Count method, but with two differences. The first one is that the efficiency ϵ_i now corresponds also to the bin selection and not only on the cuts discussed in the previous chapter. The second one is the parameter M_*, which stands for the correlation between all the bins, namely the value of M_* is the same in each $\not{E}_T$ region. The parameterization of the signal is:

$$S_i = \left[\frac{1TeV}{M_*}\right]^4 \cdot \bar{\sigma}(m_{DM}, M_{cut}) \cdot \epsilon_i(m_{DM}, M_{cut}, i) \cdot L \tag{3.19}$$

  We can notice that the parameterization is similar to 3.18, with $\mu = 1/M_*^4$ and $s_i^{EFT} = \bar{\sigma} \cdot \epsilon_i \cdot L$

- $\mathbf{\Delta S}_i$ is the new parameter we introduce to take into account that we are dealing with an underestimated signal. It is bin-dependent and it stands for the unpredicted signal. The only information we have about this parameter is that it has to be greater or equal to zero ($\Delta S_i \geq 0$).

Now we can the define the likelihood functions for each bin. We will use the same hypothesis and approximation of the the Cut and Count case, namely for each bin we will consider $\mathcal{O}_i$ and the nuisance parameter ν_i to have a Normal distribution (3.2, 3.10) and we suppose to have $\nu_i \bar{B}_i \simeq \bar{B}_i$ (3.11), whenever is possible.

The approximated likelihood function for each bin is:

$$\mathcal{L}_i(\nu_i, S_i, \Delta S_i) = \frac{1}{2\pi\sqrt{\bar{B}_i + S_i + \Delta S_i}} \frac{1}{\delta\nu_i} e^{-\frac{1}{2}\frac{(\nu_i\bar{B}_i + S_i + \Delta S_i - \mathcal{O}_i)^2}{\bar{B}_i + S_i + \Delta S_i} - \frac{1}{2}\frac{(\nu_i - 1)^2}{\delta\nu_i^2}} \tag{3.20}$$

As we did for the previous case, we will perform a profile likelihood method for the nuisance parameter ν_i. We obtain a likelihood function maximized for ν_i for each bin, which has the same form of the Cut and Count one:

$$\mathcal{L}_i(\delta\nu_i, S_i, \Delta S_i) = \frac{1}{2\pi\sqrt{\bar{B}_i + S_i + \Delta S_i}} \frac{1}{\delta\nu_i} e^{-\frac{1}{2}\frac{(\bar{B}_i+S_i+\Delta S_i-\mathcal{O}_i)^2}{\bar{B}_i^2\delta\nu_i^2+\bar{B}_i+S_i+\Delta S_i}} \tag{3.21}$$

At this point, we can define the total likelihood of our system. It will be the product of all the partial likelihood functions of each bin.

$$\mathcal{L}_{tot}(\mathbf{S}, \mathbf{\Delta S}) = \prod_{i=1}^{n} \mathcal{L}_i = \frac{1}{(2\pi)^n} \prod_{i=1}^{n} \frac{1}{\sqrt{\bar{B}_i + S_i + \Delta S_i}} \frac{1}{\delta\nu_i} e^{-\frac{1}{2}\frac{(\bar{B}_i+S_i+\Delta S_i-\mathcal{O}_i)^2}{\bar{B}_i^2\delta\nu_i^2+\bar{B}_i+S_i+\Delta S_i}} \tag{3.22}$$

where with $\mathbf{S}$ and $\mathbf{\Delta S}$ we mean the full sets of S_i and ΔS_i respectively.

The following step is the original part of this project. What one would naively think to do is to consider each ΔS_i as a nuisance parameters and then perform a profile likelihood procedure as in the case of the background error. The point in dealing with the ΔS is that we ignore its distribution, its expected value and all the other informations we used in the case of the background error. The only thing we know about ΔS_i is that it must be greater or equal to zero. This prevents us from using the profiled likelihood method because we are no more sure that the resulting test statistic χ^2 will follow a χ^2 distribution with n degrees of freedom. If ΔS_i were known, we could compute the test statistic as usual and evaluate M_*^{exc}, but this can not be done.

However, we can use the property $\Delta S_i \geq 0$ to overcome this problem. We want to set a bound on the signal which is independent on the possible values the parameter ΔS_i can take, namely a bound on M_* that holds even for the most favourable possible choice of theΔS_i. To do so, from the total likelihood in 3.22 we compute the χ^2 variable assuming that we know the values of ΔS_i. The result is

$$\chi^2 = \sum_{i=1}^{n} \frac{(\bar{B}_i + S_i + \Delta S_i - \mathcal{O}_i)^2}{\bar{B}_i^2\delta\nu_i^2 + \bar{B}_i + S_i + \Delta S_i} \tag{3.23}$$

At this point, we will choose each ΔS_i in order to minimise the χ^2 by proceeding as follows. For each bin, the value of expected background and signal $\bar{B}_i + S_i$ is calculated. We can have then two cases:

1. $\bar{B}_i + S_i \geq \mathcal{O}_i$: given that it must be positive, any value of ΔS_i will drive the likelihood away from its maximum, so in this case ΔS_i is set to zero. The physical motivation to this choice is that in this case the EFT predicted signal plus the background are enough to justify the observed number of events in that bin.

2. $\bar{B}_i + S_i < \mathcal{O}_i$: for the same reason of the previous case, ΔS_i will take the value that maximizes the partial likelihood function of the bin. The maximum value is obtained setting to zero the exponent in 3.21. So in this case we set $\Delta S_i = \mathcal{O}_i - \bar{B}_i - S_i$,

which is positive, and then permitted. The result is that we lose the bin contribution to the total χ^2, but the bin is still present in the number of degrees of freedom count. The physical reason is that in that bin EFT signal plus background are not enough to justify the observed, so it might very well be that the EFT signal is there together with an additional positive contribution from effects beyond the EFT.

At this point, we need to introduce the signal parameterization. As we briefly said before, the main point of a shape analysis is to set a correlation between the bins. In our case the evaluation is performed through the signal parameterization in 3.19. The signal S_i is different in each bin, but this is due to the different values of the cut efficiency ϵ_i, while the value of the energy scale M_* is the same for all the bins, which correlates them.

The χ^2 variable takes the form:

$$\chi^2(M_*) = \sum_{\bar{B}_i + S_i \geq \mathcal{O}_i} \frac{(\bar{B}_i + \left[\frac{1TeV}{M_*}\right]^4 \cdot \bar{\sigma} \cdot \epsilon_i \cdot L - \mathcal{O}_i)^2}{\bar{B}_i^2 \delta\nu_i^2 + \bar{B}_i} \tag{3.24}$$

The S_i in the denominator has been neglected because it is very small with respect to the background and its squared value.

The value of the lower bound on the parameter M_* is obtained as in the Cut and Count case. Our test statistic is distributed as a χ^2 with n degrees of freedom [53], so the 95 percent confidence level bound on M_* is obtained by solving:

$$\chi^2(M_*) \leq \chi^2_{95}(n) \tag{3.25}$$

The value of $\chi^2_{95}(n)$ depends on the number of bins used for the analysis and corresponds to the value of a the 0.050 percentile of a chi-square distribution with n degrees of freedom. This equation is more difficult to solve analytically, so we decided to use a numerical approach. All the details about how the value of M_*^{exc} is calculated will be discussed in the following chapter.

It is interesting to notice that the modified shape analysis is equivalent to the Cut and Count method in the case of only one bin. Indeed, the χ^2 variable becomes:

$$\chi^2 = \frac{(\bar{B} + S + \Delta S - \mathcal{O})^2}{\bar{B}^2 \delta\nu^2 + \bar{B} + S + \Delta S} \tag{3.26}$$

If we consider the signal to be contained in only one bin, the possible fluctuations of the observed are reduced, so we can impose the background-only hypothesis ($\bar{B} = \mathcal{O}$). Hence, the parameter ΔS is zero, because the condition $\bar{B} + S \geq \mathcal{O}$ is always verified. Therefore, the evaluation of the test statistic at 95% C.L. becomes:

$$\chi^2 = \frac{S^2}{\bar{B}^2\delta\nu^2 + \bar{B} + S} \leq \chi^2_{95}(1) \simeq 4 \Rightarrow S_{max} = 2 + 2\sqrt{1 + \bar{B} + \bar{B}^2\delta\nu^2} \tag{3.27}$$

as in the Cut and Count case.

3.2.2 More on ΔS

Before discussing how this statistical analysis is performed in the EFT dark matter case, we need to make some considerations about the role played by ΔS. We have to consider what happens to the variable χ^2 when the ΔS_i are evaluated. If $\bar{B}_i + S_i \geq \mathcal{O}_i$ the value of ΔS_i is set to zero, so the contribution to the χ^2 of that bin is:

$$\chi^2_i = \frac{(\bar{B}_i + \left[\frac{1TeV}{M_*}\right]^4 \cdot \bar{\sigma} \cdot \epsilon_i \cdot L - \mathcal{O}_i)^2}{\bar{B}_i^2\delta\nu_i^2 + \bar{B}_i} \tag{3.28}$$

In the other case ($\bar{B}_i + S_i < \mathcal{O}_i$), ΔS_i is set to $\mathcal{O}_i - \bar{B}_i - S_i$. In this case the contribution of the bin to the total χ^2 is zero:

$$\chi^2_i = 0 \tag{3.29}$$

This means losing all the information about that specific bin. This is consistent with what we said about our EFT model. If the signal plus background is not enough to balance the observed, that means that we are in a region were our EFT cannot predict the total true value of the signal, and so we lose all the information. In the other case, when signal plus background balance the observed, we can say that the EFT gives a good prediction, so we have maximum information and contribution to the M_*^{exc} evaluation.

Hence, the behaviour of the test statistic χ^2 is modified. The total chi-square is the sum of the contribution of all the bins:

$$\chi^2(M_*) = \sum_{i=1}^{n} \chi^2_i(M_*) \tag{3.30}$$

In the calculation of M_*^{exc} our χ^2 has to balance the 0.050 percentile of the chi-square distribution with n degrees of freedom, $\chi^2_{95}(n)$. If every bin is in the case when $\bar{B}_i + S_i \geq \mathcal{O}_i$, we have the maximum information that will lead to a certain value of M_*^{exc}. If a bin is in the opposite case its contribution to the total χ^2 is zero, so the contribution of the other bins must be higher in order to balance the value of $\chi^2_{95}(n)$. Given that every contribution χ^2_i depends on M_* to the power -4, namely $\chi^2_i \sim 1/M_*^4$, this means that the final value of M_*^{exc} will be lower.

This is an important feature that our method must have in order to be consistent. The reason is quite understandable: the more information you have, the better the value of M_*^{exc} is. In the extreme case in which every bin gives no information, namely when $\chi_i^2 = 0 \; \forall \; i = 1...n$, we cannot say anything about the value of M_*^{exc}. After this consideration, we can say that the lower bound M_*^{exc} is conservative. The value we have is always lower than value we would obtain if we knew the complete model.

As a consequence of the dependence on ΔS we cannot use the background-only hypothesis. If we suppose $\bar{B}_i = \mathcal{O}_i$ in each bin, we are always in the first case ($\bar{B}_i + S_i \geq \mathcal{O}_i$), which would mean predicting the exact value of the signal for each bin, losing the possibility for the signal to be underestimated. This does not agree with all we said before about the EFT model and which is inconsistent with the introduction of ΔS. The value of M_*^{exc} have to be calculated, though, considering some *pseudo-experiments*, namely different sets of $\mathcal{O}_i$ we suppose can be observed at LHC. We will generate a sample of pseudo-experiment and we will evaluate the value of M_*^{exc} for each one. The final result will be the mean of the partial values.

CHAPTER 4

RESULTS

In the previous chapter, our limit setting strategies has been explained and discussed. We have two possible methods and will test them in the case of our EFT dark matter model to see if the Modified Shape Analysis gives better results than the simple Cut and Count and, in this case, to set the most accurate value of the limits on the parameters. The comparison will be carried out as follows. We will start from the same point, the simulated data we have of the dark matter production process and of the neutrino background. Once we have them, both the strategies will be performed on the same samples and then the results in terms of lower bounds on M_* will be compared. We will use the best bounds to compute the closed exclusion curves in the space of the parameters by imposing the relation between the values of M_* and M_{cut} in eq. (1.6).

The last section of this chapter will be about how we can further improve our limit setting strategy by studying other types of event in addition to the mono-jet. Before showing the comparison between the two methods, the implementation of each procedure will be explained in order to understand the technical differences between them.

4.1 ERRORS

As we showed in the previous chapter, the error value of the background plays a fundamental role in both the limit setting strategies. It appears at its square power as a multiplicative factor in the denominator of the χ^2 variable and, most of the cases, it determines its value. So, in order to be the most accurate as possible, the error values used in the analysis must reproduce faithfully the CMS observations.

At the time of this work, the first 13 TeV run of LHC is already concluded, so, at our disposal, we have the data obtained in 2015 from CMS [39], reported in fig. 1.7 in sect. 1.3.2 . The background values and uncertainties are used as benchmarks for the analysis. The luminosity gathered from the detector is $L = 2.24 fb^{-1}$, which is enough for a preliminary test of the validity of our Shape Analysis method. The errors are

presented as uncertainties on the number of events with a particular $\not{E}_T$ binning decided by the CMS collaboration.

$\not{E}_T$ [GeV]	200-250	250-300	300-350	350-400	400-500	500-600	600-1000
Error $\delta\nu$	0.01	0.01	0.01	0.02	0.04	0.08	0.15

Obviously for our work we will have to adapt these values to our specific cases. For example, in the Cut and Count method we use the error on a region determined by $\not{E}_T > \not{E}_T^{min}$, so we will need the error on the region above the cut-off that will comprehend more than just one bin. Similarly, if we want use another binning for the Shape Analysis, we will have to adjust the errors. The error values adapted to our cases will be displayed in the following sections.

We are also interested in testing how the Modified Shape Analysis method will behave with a higher number of events, namely with an increased integrated luminosity L, as the total number of events is proportional to the integrated luminosity via the cross section ($N = \sigma \cdot L$). Increasing the luminosity does not only mean increasing the number of events, but it also modify the values of the background errors. Taking into account this effect is necessary to give a consistent prediction.

For our purpose, we decided to test what happens if the luminosity is increased to 100 fb^{-1}. The increased luminosity will modify sensibly the errors. To understand it, we need to make some considerations on its components. The value $\delta\nu$ is supposed to be composed by a purely systematic component σ_{sist}, which will not be affected by the increase of N, and by a statistical/systematic component σ_{stat}, that will be strongly modified if the luminosity is increased. We suppose to parameterize $\delta\nu$ as follows:

$$\delta\nu = \sqrt{\sigma_{stat}^2 + \sigma_{sist}^2} \tag{4.1}$$

As we know from the theory of errors, when the number of events is increased, the statistical component σ_{stat} is reduced by a factor $\frac{1}{\sqrt{N}}$, while σ_{sist} will remain the same. In our case, we will shift from a luminosity of 2.24 $fb^{-}1$ to 100 fb^{-1}, this means that the number of events is increased by a factor $\frac{100}{2.24} \simeq 44.6$. So the σ_{stat} will be reduced of a factor $\sqrt{44.6} \simeq 6.8$ and the total error will be:

$$\delta\nu' = \sqrt{\sigma_{sist}^2 + \frac{\sigma_{stat}^2}{44.6}} \tag{4.2}$$

The problem about this procedure is that the components of the error are not given, but we know only the total value $\delta\nu$ at 2.24 fb^{-1}. This means we have to make an assumption on the possible value of the systematic error in order to compute σ_{stat} and then project it to 100 fb^{-1}. We suppose that until $\delta\nu$ is less than 0.05, the systematic and

the statistical components give the same contribution to the total error, but when $\delta\nu$ goes beyond 0.05, the σ_{sist} value is then fixed to 0.05. Under these assumptions, from the $\delta\nu$ values at 2.24 fb^{-1} we can calculate the components σ_{sist} and σ_{stat}. We can obtain a projection of the errors $\delta\nu'$ at 100 fb^{-1} rescaling the statistical component by a factor $\sqrt{44.6}$.

Therefore, the error will be slightly reduced in the first bins, when σ_{sist} and σ_{stat} have the same weight, but when $\delta\nu$ goes beyond 0.05, the value of $\delta\nu'$ will be fixed by $\sigma_{sist} = 0.05$, because σ_{stat} is killed by the statistical scaling factor, as it is shown in eq. (4.2). This will obviously improve the knowledge of the high $\not{E}_T$ region, where the error at 2.24 fb^{-1} is mainly due to the low number of events. After these fundamental considerations about the error, we can show the results obtained with the two procedures and compare them.

4.2 Cut and Count results

In this section we will show and explain the result obtain from our data with the Cut and Count method. We will include the error on the background value treated as a nuisance parameter. First of all, we need to choose the lower values of $\not{E}_T$ that will define our Signal Regions. Moreover, we have to compute all the parameters involved to M_*^{exc} calculation for each region, namely the background value $\bar{B}$, the total error $\delta\nu_{SR}$ and the excluded cross section σ_{exc}. We need also, after the value of M_{cut} is fixed, to compute the efficiency ϵ_{SR} of the cuts for the each dark matter simulation restricted to the signal region.

Once we have all this information, we can compute the lower bound on M_* for each Signal Region and for each dark matter mass and then decide which is the best signal region for a fixed M_{cut}. To obtain the background value of a given signal region is enough to impose a further condition on the minimum value of $\not{E}_T$ in the event selection.

The value of the total error on the background of the signal region $\delta\nu_{SR}$ is calculated as an average of the errors of the bins included in it, weighted with the number of events of each bin. This means that the most populated bins, namely the low $\not{E}_T$ ones, will determine the value $\delta\nu_{SR}$. The excluded cross section is calculated dividing the maximum extra-signal value computed in 3.14 by the luminosity.

We start with the low-luminosity case $L = 2.24\ fb^{-1}$. In the following table the parameters of the background analysis are displayed.

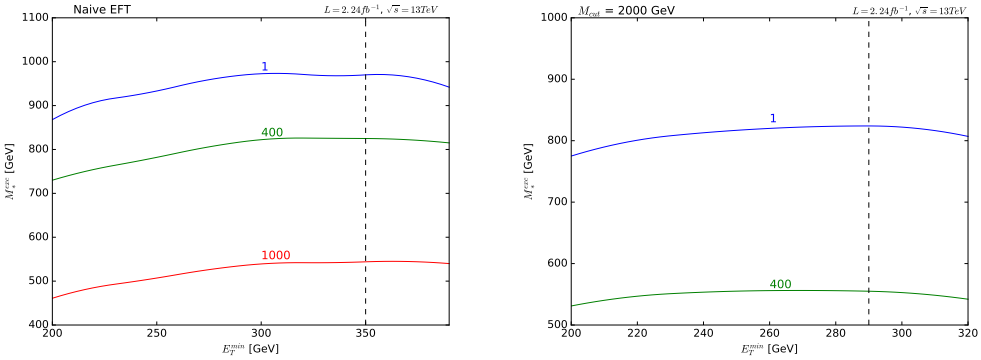

Figure 4.1: This two images represent the value of M_*^{exc} depending on the $\not{E}_T$ cut-off for different dark matter masses. The vertical dashed line represents the optimal region $\not{E}_T^{min}$.

L = 2.24 fb^{-1}			
$\not{E}_T$ [GeV]	$\delta\nu_{SR}$	$\bar{B}$	σ_{exc} [pb]
> 200	0.011	60878	0.64
> 230	0.012	34332	0.40
> 260	0.014	19937	0.28
> 290	0.016	12020	0.20
> 320	0.020	7481	0.16
> 350	0.026	4808	0.13
> 390	0.037	2806	0.10

In figure 4.1 we can see how the value of the lower bound on M_* changes with the minimum value of $\not{E}_T$. We can notice two important things from the two images. The first one is the optimal signal region does not depend on the dark matter mass m_{DM}, but only on the value of M_{cut}, so we can consistently define one region for each M_{cut} value. The second one is that the optimal cut-off on $\not{E}_T$ lowers when M_{cut} is lowered. This can be explained intuitively, lowering M_{cut} means reducing the energy budget of the process, so, to obtain an optimal number of events, the $\not{E}_T$ cut-off must be lowered to allow the production of the dark matter particle in addition to the light jet. We can also notice that in the right panel there is not the $m_{DM} = 1000$ GeV line. This happens because M_{cut} is to low to produce a pair of dark matter particle plus the jet.

In the following table the optimised signal region for each M_{cut} value are displayed.

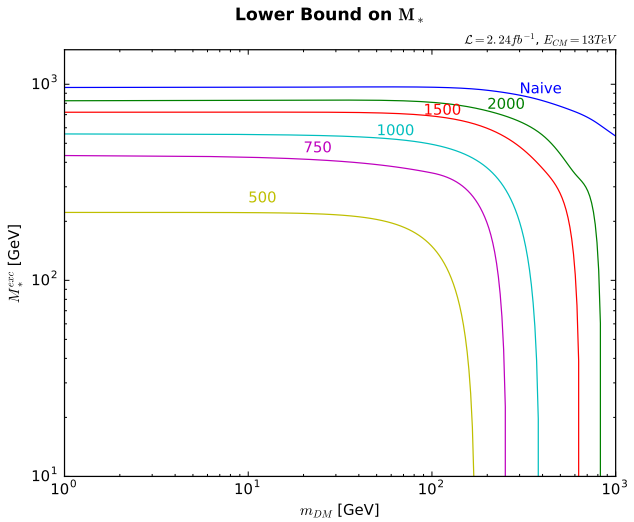

Figure 4.2: Lower bound on M_* obtained with cut and count method with an integrated luminosity of 2.24 fb^{-1}. Each curves corresponds to a M_{cut} value.

L = 2.24 fb^{-1}							
$\mathbf{M_{cut}}$	500	750	1000	1500	2000	4000	13000
$\not{E}_\mathbf{T} >$	200	200	200	230	290	320	350

The values of M_{cut} and $\not{E}_T$ are expressed in GeV.

Now the we have the optimised signal regions, we can compute the value of M_*^{exc} for each value of the dark matter mass. The lower bounds we obtain are plotted in 4.2.

We can notice that each curve corresponding to $M_{cut} < 2000$ GeV has an endpoint at a given m_{DM}. This property is due to the fact that limiting the maximum value of the centre of mass of the process reduces the energy budget for the dark matter production. To be more specific, we need to produce a couple of dark matter particles with a given mass plus one jet. These two particles must balance at least 200 GeV of $\not{E}_T$ and the jet must have a minimum p_T^{jet} value of 150 GeV, so, once M_{cut} is fixed, if the dark matter particles are too heavy, they cannot be produced in the collider. The cut efficiency drops to zero and kills the signal in acceptance, as we said when we discussed the behaviour of the ϵ value in 2.3.1 .

We recall the expression for the maximum dark matter mass value from M_{cut} and the cut-off on $\not{E}_T$:

$$m_{DM}^{max} = \frac{M_{cut}}{2}\sqrt{1 - 2\frac{\not{E}_T}{M_{cut}}} \tag{4.3}$$

We can now extend the procedure to the 100 fb^{-1} integrated luminosity case. To do so, we need to calculate the projection of the error values, as we discussed in the previous section. We need also to compute the new background values, which will be 44.6 times bigger than the 2.24 fb^{-1} case.

After these considerations, we can compute the values of σ_{exc} in each signal region.

L = 100 fb^{-1}			
$\not{E}_T$ [GeV]	$\delta\nu_{SR}$	B	σ_{exc} [pb]
> 200	0.008	2717808	0.44
> 230	0.009	1532655	0.27
> 260	0.010	890042	0.18
> 290	0.012	536600	0.13
> 320	0.014	333967	0.10
> 350	0.018	214628	0.08
> 390	0.026	125288	0.06

We can notice that the values of σ_{exc} are lower than the 2.24 fb^{-1}. As we said in the previous chapter, the excluded cross section σ_{exc} represents the maximum cross section compatible with the background within its error at 95% of confidence level. At 100 fb^{-1} the error on B is lower and so its possible fluctuations. We expect, then, the excluded cross section to be lower than in the previous case. This improved knowledge of the background will lead to a better M_*^{exc} value.

To obtain the new lower bound, an evaluation of the optimal signal region is needed with the new parameters. We noticed, though, that the optimal SR at 100 fb^{-1} are the same of the previous case, even if the M_*^{exc} are different.

The result obtained with this method at 100 fb^{-1} are displayed in 4.3. As we expect, the value of the M_*^{exc} are increased. This is due to the better information we have about the background. With this improved statistic, the Cut and Count method appears to be too rough. With the signal region selection, we do not consider a lot of information that could be used for a better evaluation of M_*^{exc} because now the errors are lower and our precision is increased, so the excluded signals can contribute more efficiently than in the 2.24 fb^{-1} case.

In the next section we will se how the Modified Shape Analysis will provide for this lack of the Cut and Count method, obtaining an optimised value for the lower bound on M_*.

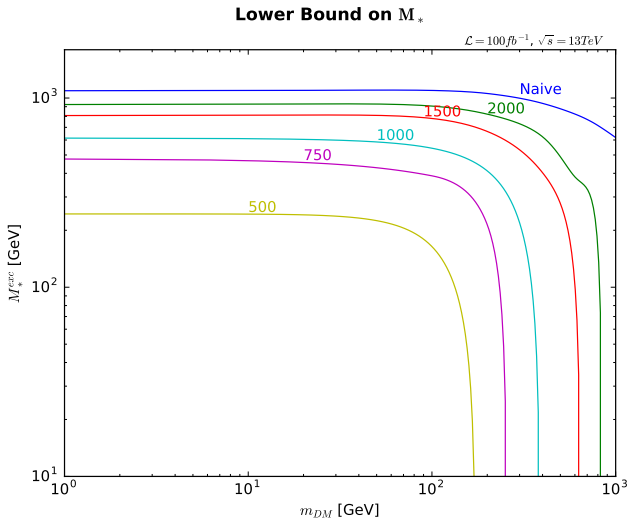

Figure 4.3: Lower bound on M_* obtained with cut and count method with an integrated luminosity of 100 fb^{-1}. Each curves corresponds to a M_{cut} value.

4.3 Modified Shape Analysis results

In the previous section the results of the Cut and Count method was presented. We said that it is a consistent method that allows us to set a conservative lower bound on the parameter M_* of the theory. Now we will show the results of the Shape Analysis. As we will see, this method improves the value of M_*^{exc} even in the low-luminosity case (2.24 fb^{-1}).

4.3.1 Pseudo Experiment

Before discussing the full results and the comparison between the two methods, we need to explain the concept of pseudo-experiments and why we need to use them for the Modified Shape Analysis. A pseudo-experiment is a set of binned background values that are compatible with the true value of background measured by the CMS detector. As a consequence, we can imagine we have at our disposal more than one background samples with the same characteristics of the true one.

In the case of the Shape Analysis this is necessary because it is based on the evaluation case by case of the signal and background values, so it is strictly dependent on their fluctuations. As we said in the previous chapter, the theoretical reason is that we cannot use the background-only hypothesis because it is inconsistent with the introduction of ΔS. For a consistency reason, the mean value obtained with the ΔS parameter must be always lower the the mean value we would have obtained without its introduction.

To generate the Pseudo-Experiments we need the true value of the background for

each bin we have from the CMS detector. To generate the sample, the *numpy.random* library of python is used. We suppose that the background have a Normal distribution around the true value with the standard deviation given by:

$$\sigma_i = \sqrt{\bar{B}_i + \delta\nu^2 \bar{B}_i^2} \tag{4.4}$$

This method with provide us a sample of possible backgrounds. For each one, we will compute the value of M_*^{exc} using the Shape Analysis and then the final value will be the mean of all the partial values. In our particular case, we generated 30 pseudo-experiments on which calculate M_*^{exc}. Given that the generated values depends only on the background, to be consistent we will use the same sample of 30 pseudo-experiments to calculate all the bounds with different M_{cut} and m_{DM}. We will generate a sample for the 2.24 fb^{-1} case and one for the 100 fb^{-1} case.

4.3.2 Comparison

Now we will discuss the details and the results of the Shape Analysis with the current data at $L = 2.24 fb^{-1}$ and with the projection at $L = 100 fb^{-1}$. We decided to divide the events in 14 bins with different widths in order to lower the fluctuations in the high $\not{E}_T$ zone. This means that the χ^2-variable will be distributed as a χ^2 with 14 degrees of freedom, so the 0.050 percentile of the distribution is $\chi^2_{95}(14) \simeq 24$. Once m_{DM} and M_{cut} are fixed, for each bin we need to know the background value $\bar{B}_i$, the error on the background $\delta\nu_i$, the value of observed generated with the pseudo-experiment $\mathcal{O}_i$ and the efficiency on the dark matter signal restricted to the bin ϵ_i.

We use a numerical approach to solve the equation given by eq. (3.25) to obtain the value of M_*^{exc} for each combination of M_{cut} and m_{DM}. We can notice that our χ^2-variable in eq.(3.24) depends on the value M_* to the power -4 ($\sim 1/M_*^4$), so for a low value of M_* our χ^2 will be surely higher than the threshold $\chi^2_{95}(14)$. When M_* is increased, the value of the total χ^2 lowers until it reaches the limit value.

Our numerical approach consists in increasing the value of M_* following steps of 1 GeV each until the total χ^2 reaches the value of $\chi^2_{95}(14)$. At that point the value of M_* will be the exclusion lower bound with the precision of 1 GeV. Within this procedure we can also deal with the ΔS parameter. As we said before, the effect of ΔS on the contributions χ_i^2 is to erase them or leave them unchanged, so, for the numerical approach, we need to introduce a simple parameterization of the contributions:

$$\chi_i^2 = \frac{(\bar{B}_i + \left[\frac{1TeV}{M_*}\right]^4 \cdot \bar{\sigma} \cdot \epsilon_i \cdot L - \mathcal{O}_i)^2}{\bar{B}_i^2 \delta\nu_i^2 + \bar{B}_i} \cdot f_i \tag{4.5}$$

where f_i is a step function that can be one or zero, depending on the value of ΔS_i.

$$\begin{array}{lll} \bar{B}_i + S_i \geq \mathcal{O}_i & \rightarrow & \Delta S_i = 0 \qquad\qquad\quad \rightarrow \quad f_i = 1 \\ \bar{B}_i + S_i < \mathcal{O}_i & \rightarrow & \Delta S_i = \mathcal{O}_i - \bar{B}_i - S_i \quad \rightarrow \quad f_i = 0 \end{array}$$

With this parameterization the result is the same, but easier to implement in the code.

The only thing left to do is the evaluation of ΔS_i. For the first step we suppose to have $f_i = 1 \ \forall i = 1...n$ (this hypothesis does not change in anyway the final result). After the first evaluation of the total χ^2, the values of f_i are calculated following the prescriptions for ΔS, the value of M_* is increased by 1 GeV and the cycle restarts. This code is stable and provides us the value of M_*^{exc} we need.

At this point, we have to to set the parameters for the calculations. The details of the binning are displayed in the following table.

L = 2.24 fb^{-1}

$\not{E}_T$ [GeV]	$\delta\nu_i$	$\bar{B}_i$
200-230	0.01	26548
230-260	0.01	14394
260-290	0.01	7917
290-320	0.01	4539
320-350	0.01	2673
350-390	0.01	2001
390-430	0.02	1107
430-470	0.03	643
470-510	0.04	385
510-550	0.05	201
550-640	0.06	269
640-740	0.08	126
740-900	0.12	57
> 900	0.22	17

The values of the $\bar{B}_i$ column are used as mean values to generate the pseudo-experiments. Now that we have all the parameters set, we can proceed to the results of the Shape Analysis on our dark matter EFT model. The comparison between the lower bound values on M_* obtained with the two methods is shown in 4.4.

As we can see, the Shape Analysis provides in any case a stronger value of M_*^{exc} than the Cut and Count method. The parameter used to describe the performance of the methods is, for fixed m_{DM} and M_{cut}, the ratio between the values of M_*^{exc} at the 4^{th} power, namely:

$$R = \left(\frac{M_*^{SA}}{M_*^{CC}} \right)^4 \tag{4.6}$$

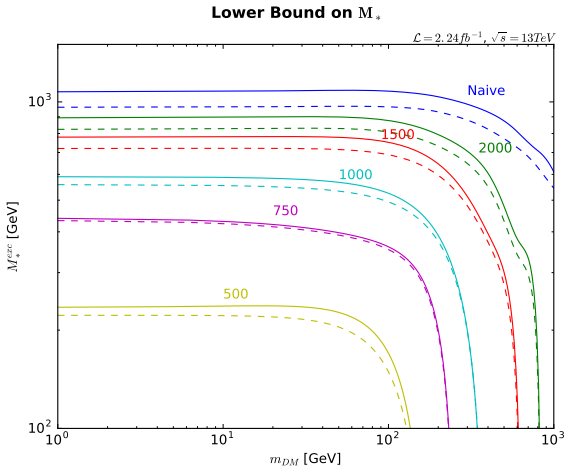

Figure 4.4: In the figure the lower bounds on M_* are presented. The solid lines correspond to the Shape Analysis while the dashed lines refer to the Cut and Count result of the previous section.

where "SA" refers to Shape Analysis and "CC" to Cut and Count. For the naive EFT with $m_{DM} = 100$ GeV the maximum value of R is obtained ($R = 1.56$), while the minimum value is given by $m_{DM} = 1$ GeV and $M_{cut} = 750$ GeV (R = 1.07). We proved the our particular Shape Analysis is more performing than the Cut and Count method even with a low number of events, when it is suppose to be more effective. We expect, then, that in the projection at 100 fb^{-1} the increased knowledge of the background will make the Shape Analysis even more performing at the expense of the Cut and Count method.

In the following table the details of the 100 fb^{-1} background are displayed.

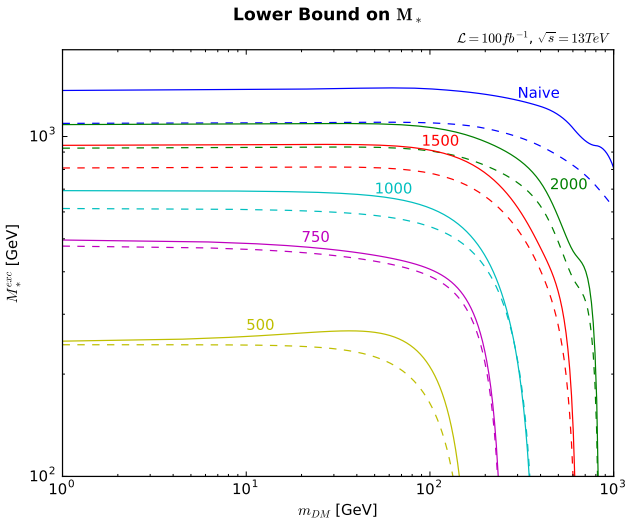

Figure 4.5: In the figure the lower bounds on M_* are presented. The solid lines correspond to the Shape Analysis while the dashed lines refer to the Cut and Count result of the previous section.

L = 100 fb^{-1}		
$\not{E}_T$ [GeV]	$\delta\nu_i$	$\bar{B}_i$
200-230	0.007	1185178
230-260	0.007	643610
260-290	0.007	353449
290-320	0.007	202642
320-350	0.007	119338
350-390	0.007	89340
390-430	0.014	49402
430-470	0.022	28702
470-510	0.029	17188
510-550	0.036	8987
550-640	0.050	12020
640-740	0.051	5645
740-900	0.052	2556
> 900	0.060	702

The errors $\delta\nu_i$ are lower than before, especially in the high-$\not{E}_T$ zone, where the main component is the systematic set to 0.05.

In figure 4.5 the comparison between the two method at $L = 100 fb^{-2}$ is shown.

As we can see, not only the values of M_*^{exc} are higher, but also the performance of

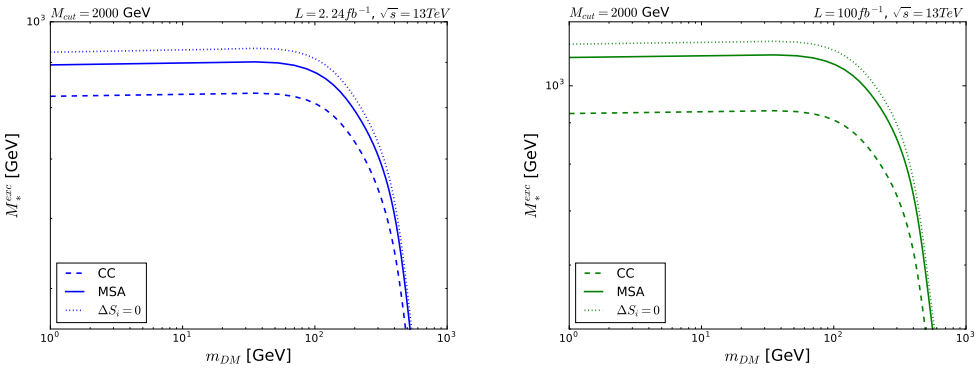

Figure 4.6: The figure shows the comparison between the limit set with the Cut and Count (CC), the Modified Shape Analysis (MSA) and the Usual Shape Analysis ($\Delta S_i = 0$) for a fixed $M_{cut} = 2000$ GeV. The result is presented for $L = 2.24 fb^{-1}$ (left panel) and for $L = 100 fb^{-1}$ (right panel).

the Shape Analysis are sensibly increased. For a $m_{DM} = 100$ GeV within the naive EFT the performance ratio is $R = 2.52$ instead of 1.52 of the previous case.

In fig. 4.6, in addition to the limits obtain with the Cut and Count and with the Modified Shape Analysis, the M_*^{exc} curve is plotted also in the case of Shape Analysis without the introduction of the parameter ΔS for a fixed $M_{cut} = 2000$ GeV. As we expected, the limit on M_* is stronger if ΔS is not considered, however, the MSA limit is more conservative because it accounts for the possible signal excess due to fact that we ignore the underlying UV model. Indeed, the introduction of ΔS would not be necessary only if we knew the complete microscopic model. However, the fact that MSA limit is always lower than the one without ΔS provides another evidence of the consistency of our statistical method.

After these considerations, we can say that the Modified Shape Analysis is more performing and provides better lower bounds than the Cut and Count in any regime of statistics (low and high number of events). It solves the problem of the loss of information due to the selection of the $\not{E}_T$ optimal region, which is used to improve the lower bound calculation. In the next section we will use the results of the Shape Analysis to build the exclusion curves at fixed g_*.

4.4 Exclusions at Fixed Coupling

In this section we will recall the hypothesis made in the first chapter of a relation between the parameters M_{cut} and M_*. The relation we are talking about is the following:

$$M_{cut} = g_* M_* \tag{4.7}$$

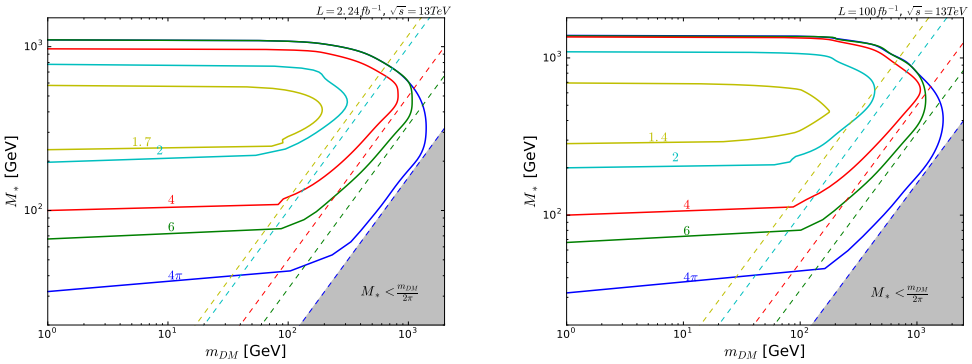

Figure 4.7: The closed exclusion curves are displayed for 2.24 fb^{-1} and 100 fb^{-1}. The dashed lines corresponds to the kinematically forbidden zone for each g_* value.

where g_* is the coupling strength of the underlying microscopic theory. We can use this relation to see how much of the allowed parameter space is actually tested by our analysis. A priori, g_* could take any value, but we can make some considerations to limit it. First of all, in order to keep our theory perturbative it must be that $g_* < 4\pi$, which implies an upper bound on M_{cut} for any fixed M_*. The second consideration is that we are treating a WIMP-like theory, so we expect $g_* \simeq 1$. The effect of eq. (4.7) in the limit setting is to "close" the exclusion curves with a low-M_* limit. This can be easily understand. For a fixed g_* value, lowering M_* means lowering also M_{cut}, and this can lower too much the signal in acceptance or even kill it. So, the limit must disappear also for low values of M_*.

The low-M_* limit is calculated as follows. The minimum centre of mass energy to create a couple of dark matter particles plus jet is:

$$E_{CM}^{min} = \not{E}_T + \sqrt{(\not{E}_T)^2 + 4m_{DM}^2} \tag{4.8}$$

where $\not{E}_T$ is the minimum value for the mono-jet event selection (200 GeV). We identify E_{CM}^{min} with the limit value of M_{cut} and from eq. (4.7) we obtain the low-M_* limit.

This consideration also lead to the consequence that there is a zone of our parameter space which is forbidden. It happens because in order to produce a pair of dark matter particles we need at least $M_{Cut} > 2m_{DM}$, but with 4.7 this correspond to $M_* > \frac{2m_{DM}}{g_*}$. This means that in the region where $M_* < \frac{2m_{DM}}{g_*}$ no dark matter can be produced, even if $m_{DM} = 0$. The exclusion curves are shown in 4.7 for fixed values of g_*.

In this figures we can see how much of the allowed parameter space is actually explored by our analysis. The more the exclusion curve is near to its kinematical limit

(dashed line), the better the parameter space is explored. As we can notice, this target is achieved, especially in the case of $L = 100 fb^{-1}$. The curves are very close to their limit for most of the g_* values.

The other target of this kind of analysis is to test the low g_* zone ($g_* \simeq 1$). This topic is strictly connected with the sensitivity of our experiment. As we can see from the figures, the lowest value of g_* we can test is 1.4 in the $L = 100 fb^{-1}$, which is a good result. If we want to improve the sensitivity, a low-M_{cut} analysis is needed.

It is difficult, tough, to test the g_* values near to 1 because choosing $g_* = 1$ means that $M_{cut} = M_*$, a condition difficult to obtain because it is supposed to happen with low values of M_{cut}. This means low E_{CM} for the processes that make difficult or even impossible to obtain enough signal in acceptance to perform the analysis. This is mainly due to the mono-jet event selection cuts.

4.5 OUTLOOK

Supposing a relation between M_* and M_{cut} we are able to improve the precision and the exclusion power of our analysis. Nevertheless, the dependence of the low-M_* limit on the minimum $\not{E}_T$ in eq. (4.8) forces the bound to by higher. For example, in a similar analysis at 8 TeV shown in fig. 4.8, we can see that even if the high-M_* bound provided by our analysis is stronger than the 8 TeV analysis because of the improved performance of LHC and of our statistical method, the low-M_* exclusion bound is stronger in the 8 TeV analysis because the $\not{E}_T$ acceptance-cut is at 120 GeV for the mono-jet category. This means that our exclusion power in the low-M_* zone is not limited by the performance of the experiment or by the statistical analysis, but by the category of the event we decided to choose. This is a bound we cannot overcome with any means if we want to use mono-jet events.

One possible solution could be choosing another category of events for our dark matter search. We will need a type of events that requires a minimum $\not{E}_T$ or p_T lower than the mono-jet, for example the mono-photon [55]. The mono-photon event signature consists in the presence of a large amount of $\not{E}_T$ plus an energetic photon with a minimum transverse momentum of p_T of 145 GeV. However, this kind of event has a lower cross section than the mono-jet and this means that the value of the high-M_* limit will be worse than what we have now obtained with the mono-jet analysis. Therefore, improving the low-M_* would mean deteriorate the high-M_* one. A proper discussion of this topic is needed in order to understand which is the best choice for this kind of analysis.

Another improvement for the Modified Shape Analysis could be the introduction of a more specific likelihood for the events. In our case, we decided to approximate the true Poisson distribution of the events with a Normal distribution under the assumption of a large number of events for each bin. For our interpretation of the mono-jet events this is always verified, even at high $\not{E}_T$ regions, but this could not always happen with other kinds of events. A proper binning is also required to improve the power of our analysis.

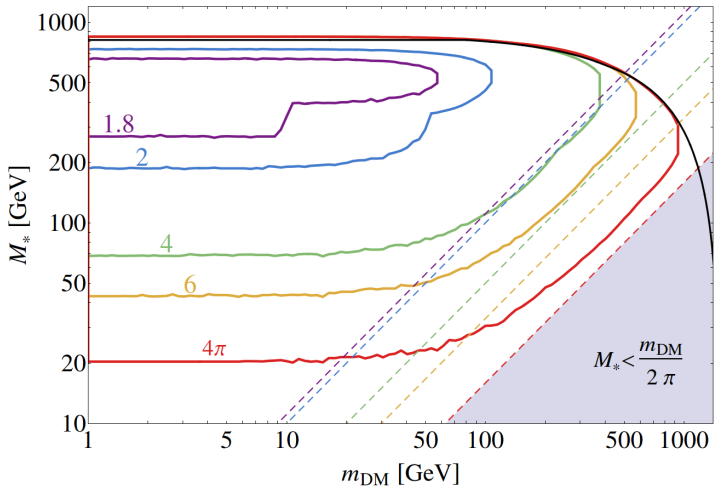

Figure 4.8: The figure shows a previous result in terms of exclusion curves at fixed g_* obtained by a similar analysis [24].

With a few bins, we have more stable values and the risk for the gaussian approximation to fail is low, but the approximated event distribution can be too rough and the results could not be much better than a Cut and Count. On the other hand, with a lot of bins the performance is increased, but the gaussian approximation can fail in the high-$\not{E}_T$ region and therefore warp the results.

CONCLUSIONS

We described a new statistical method to set universal bounds on the production of heavy-mediator Dark Matter at the LHC based on the Effective Field Theory approach. To describe the interaction between dark matter particles (Majorana fermion) and ordinary matter we chose a dimension 6 axial-axial effective operator. We decided to focus on the CMS mono-jet analysis to test the effectiveness of our EFT approach and of the statistical method we propose. We accurately simulated the EFT signal and the mono-jet background using a chain of Monte Carlo based softwares that accounts for the full simulation from the hard scattering to the detector response. The signal was simulated for different values of the DM mass m_{DM}, while we reproduced the background simulating the $Z(\nu\nu)$ and $W(\nu l)$ components, which constitute most of the total mono-jet background. After the simulation was performed, we selected the mono-jet events obtaining the efficiencies of the cuts. Moreover, for the signal we decided a strategy to set the theoretical cut on the invariant mass of the process in order to study the limited range of validity that characterise the effective theories.

To set bounds on the parameters of the EFT we used the Cut and Count method. This method is based on the assumption that the EFT underestimates systematically the true value of the signal. For each value of m_{DM} and M_{cut} we selected the proper signal region and calculate the limit by imposing that the EFT cross section in that region is lower the the maximum cross section allowed by the background with 95% C.L. For a more refined limit-setting analysis, we decided to test a new statistical method, the Modified Shape Analysis (MSA), which is based on the principle that we can use the events distribution of the signal predicted by the EFT as a lower bound on the distribution of the true signal, namely the one we would obtain if we knew the complete microscopic theory. Improving the performance of the statistic method implies improving, without loosing the model-independence, the power or the EFT approach to discriminate the validity of the multitude of possible microscopic models which can generate the effective operator.

The improved performance of the MSA can be seen in the exclusion curves at fixed g_*. The exclusion power is greater and we are able to test a larger region of the theoretically allowed parameter space. Moreover, we have more sensitivity to the low-g_* region ($g_* \simeq 1$) that can be further improved with a dedicated low-M_{cut} analysis. Another important feature of the MSA method is that is general, and it can be also applied in other situations where we want to test the validity of a theory but we have at our

disposal only an underestimation of the signal. Obviously, this is only a coarse version of the method. Many improvements can be done, such as the usage of a proper binning to obtain the maximum information from the data or the choice of a more accurate likelihood function for the event distribution, but the fact that even in this preliminary version the performance are clearly improved makes us hope for future applications in particle physics.

BIBLIOGRAPHY

[1] L.E. Stringari, *Galactic searches for dark matter*, Physics Reports 531 (2013) 1-88, arXiv:1211.7090.

[2] G. Bertone, D. Hooper, J. Silk, *Particle dark matter: evidence, candidates and constraints*, Physics reports 405 (2005) 279-390, arXiv:hep-ph/0404175

[3] J. L: Feng, *Dark matter candidates from particle physics and methods of detection*, Ann. Rev. Astron. Astrophys. 48 (2010) 495, arXiv:1003.0904

[4] Plank Collaboration, *Plank 2013 results.XVI. Cosmological parameters*, arXiv:1303.5076.

[5] D. Clowe et al., *A direct empirical proof of the existence of dark matter*, Astrophys. j. 648 (2006) L109, arXiv:astro-ph/0608407

[6] S. Dodelson, *Modern Cosmology*, Burlington, Academic Press (2003)

[7] E. W. Kolb, M. S. Turner, *The early universe*, Redwood City, Addison-Wesley (1990)

[8] D. Whitestone, *Dark Matter Collider Searches*, Lectures given at the 42nd SLAC Summer Institute, Stanford, USA, 4-15 August 2014

[9] M. E. Peskin, D. V. Schroeder, *An Introduction to Quantum Filed Theory*, Westview Press

[10] M. W. Goodman and E. Witten, *Detectability of Certain Dark Matter Candidates*, Phys. Rev. D 31 (1985) 3059.

[11] A. Birkendal, K. Matchev and M. Perestein, *Dark Matter at colliders: A Model Independent approach*, Phys. Rev. D 70 (2004) 077701 [hep-ph].

[12] M. Beltran et al., *Deducing the nature of dark matter from direct and indirect detection experiments in the absence of of collider signatures of new physics*, Phys. Rev. D 80 (2009) 043509 [arXiv:0808.3384[hep-ph]].

[13] Q. H. Cao, C. R. Chen, C. S. Li and H. Zang, *Effective Dark Matter Model: Relic Density*, CDMS II, Fermi LAT and LHC, JHEP 1108 (2011) 018 [arXiv:0912.4511[hep-ph]].

[14] M. Beltran, D. Hooper, E. W. Kolb and Z. C. Krusberg and T.M.P. Tait, *Maverick dark matter at colliders*, JHEP 1009 (2010) 037 [arXiv:1002.4137[hep-ph]].

[15] J. Goodman, M. Ibe, A. Rajamaran, W. Shepherd, T.M.P. Tait and H.B. Yu, *Constraints on Light Majorana Dark Matter from Colliders*, Phys. Lett. B 695 (2011) 185 [arXiv:1005.1286 [hep-ph]].

[16] Y. Bai, P. J. Fox and R. Harnik, *The Tevatron at the Frontier of Dark Matter Direct Detection*, JHEP 1012 (2010) 048 [arXiv:1005.3797[hep-ph]].

[17] A. Rajamaran, W. Shepherd, T.M.P. Tait and A. M. Wijangco, *LHC Bounds on Interactions of Dark Matter*, Phys. Rev. D 84 (2011) 095013 [arXiv:1108.1196[hep-ph]].

[18] J. Goodman, M. Ibe, A. Rajamaran, W. Shepherd, T.M.P. Tait and H.B. Yu, *Constraints on Dark Matter from Colliders*, Phys. Rev. D 82 (2010) 116010 [arXiv:1008.1783 [hep-ph]].

[19] P. J. Fox, R. Harnik, J. Kopp and Y. Tsai, *Missing Energy Signatures of Dark Matter at LHC*, Phys. Rev. D 85 (2012) 056011 [arXiv:1109.4398[hep-ph]].

[20] A. Crivellin, F. D Eramo and M. Procura, *New Constraints on Dark Matter Effective Theories from Standard Model Loops*, Phys. Rev. Lett. 112 (2014) 191304 [arXiv:1402.1173 [hep-ph]].

[21] S. Davidson, *Including the Z in an Effective Field Theory for dark matter at the LHC*, JHEP 1410 (2014) 84 [arXiv:1403.5161[hep-ph]].

[22] F. D Eramo and M. Procura, *Connecting Dark Matter UV Complete Models to Direct Detection Rates via Effective Field Theory*, arXiv:1411.3342 [hep-ph].

[23] M. Duch, B. Grzadkowsky and J. Wudka, *Classification of effective operators for interactions between the Standard Model and dark matter*, arXiv:1412.0520 [hep-ph].

[24] D. Racco, A. Wulzer, F. Zwirner, *Robust collider limits on heavy-mediator Dark Matter*, arXiv:1502.04701v3 [hep-ph].

[25] D. G. Cerdeno, A. M. Green *Direct detection of WIMPs*, published in G. Bertone (ed.), *Particle dark matter: observations, models and searches*, Cambridge, Cambridge University Press (2010)

[26] O.S.Bruning, P.Collier, P.Lebrunetal et al., *LHC Design Report*, CERN, Geneva 2004.

[27] CMS Collaboration, *The CMS experiment at the CERN LHC*, JINST 3 (2008) S08004

[28] CMS Collaboration, *Precise mapping of the magnetic field in the CMS barrel yoke using cosmic rays*, Journal of Instrumentation 5 (2010), no. 03, T03021.

[29] CMS Collaboration, *Particle-Flow Event Reconstruction in CMS and Performance for Jets, Taus, and $\not\!\!E_T$*, CMS-PAS-PFT-09-001 (2009).

[30] CMS Collaboration, *Commissioning of the Particle-flow Event Reconstruction with the first LHC collisions recorded in the CMS detector*, CMS-PAS-PFT-10-001 (2010).

[31] CMS Collaboration, *Description and performance of track and primary-vertex reconstruction with the CMS tracker*, JINST 9 (2014), arXiv:1405.6569.

[32] CMS Collaboration, *Energy Calibration and Resolution of the CMS Electromagnetic Calorimeter in pp Collisions at $\sqrt{s}$ = 7 TeV*, JINST 8 (2013) P09009, arXiv:1306.2016.

[33] CMS Collaboration, C. Collaboration, *The CMS hadron calorimeter project: Technical Design Report*, Technical Design Report CMS. CERN, Geneva, 1997.

[34] CMS Collaboration, CMS, *The CMS muon project: Technical Design Report*, Technical Design Report CMS. CERN, Geneva, 1997.

[35] CMS Collaboration, *Performance of CMS muon reconstruction in pp collision events at $\sqrt{s}$ = 7 TeV*, Journal of Instrumentation 7 (2012), no. 10, P10002.

[36] CMS Collaboration, *Search for dark matter and large extra dimensions in mono-jet events in pp collisions at $\sqrt{s}$ = 7 TeV*, JHEP 1209 (2012) 094, arXiv:1206.5663

[37] CMS Collaboration, *Search for new physics in monojet events in pp collisions at $\sqrt{S}$ = 8 TeV*, CMS PAS EXO 12-048

[38] The CMS Collaboration, *Search for new physics in the V/jet + MET final state*, CMS PAS EO-12-055

[39] The CMS Collaboration, *Search for dark matter with jets and missing transverse energy at 13 TeV*, CMS-PAS-EXO-15-003, December, 2015

[40] The CMS Collaboration, *Performance of Missing Transverse Momentum Reconstruction Algorithms in Proton-Proton Collisions at $\sqrt{s} = 8$ TeV with the CMS Detector*, CMS PAS JME-12-002

[41] The CMS Collaboration, *Performance of the Jet-Plus-Tracks algorithm in Run I*, CMS PAS JME 14-005

[42] J. Alwall, M. Herquet, F. Maltoni, O. Mattelaer, T. Stelzer, *MadGraph 5: Going Beyond*, arXiv:1106.0522v1 [hep-ph].

[43] C. Degrande, C. Duhr, B. Fuks, D. Grellscheid, O. Mattelaer, and T. Reiter, *Ufo - the universal feynrules output* .

[44] F. Maltoni and T. Stelzer, *MadEvent: Automatic event generation with MadGraph*, arXiv:0208156v1[hep-ph].

[45] E. Boos et. al.,*Generic user process interface for event generators*, arXiv:0109068v1[hep-ph].

[46] J. Alwall et. al., *Comparative study of various algorithms for the merging of parton showers and matrix elements in hadronic collisions*, arXiv:0706.2569[hep-ph]

[47] R. K. Ellis, W. J. Stirling, B. R. Webber, *QCD and collider physics*, Cambridge Monographs on particle physics, nuclear physics and cosmology

[48] T. Sjostrand, S. Mrenna, P. Skands, *Pythia 6.4 physics and manual*, iopscience:jhep05(2006)026

[49] M. Cacciari, G. Salam, G. Soyez, *The anti-k_t jet clustering algorithm*, arXiv:0802.1189v2 [hep-ph].

[50] J. de Favereau et al., *Delphes 3, a modulare framework for fast simulation of a generic collider experiment*, arXiv:1307.6346v3

[51] , *Root tree description*, https://cp3.irmp.ucl.ac.be/projects/delphes/wiki/WorkBook

[52] W. A. Rolke, A. M. Lopez, J. Conrad, *Limits and Confidence Intervals in the Presence of Nuisance Parameters*, arXiv:physics/0403059v5 [physics.data-an]

[53] K.A. Olive et al. , *Particle Data Group/STATISTIC*, Chin. Phys. C, **38**, 090001 (2014) and 2015 update.

[54] G. Cowan, *Statistical Data Analysis*, Oxford Science Publications.

[55] The CMS Collaboration, *Search for Dark Matter and Large Extra Dimensions in pp Collisions Yielding a Photon and Missing Transverse Energy*, arXiv:1204.0821v2 [hep-ex]